The emergence and evolution of gene expression in genome regions replete with regulatory motifs

Timothy Fuqua[1,2], Yiqiao Sun[1,2], Andreas Wagner[1,2,3*]

ABSTRACT

Gene regulation is essential for life and controlled by regulatory DNA. Mutations can modify the activity of regulatory DNA, and also create new regulatory DNA, a process called regulatory emergence. Non-regulatory and regulatory DNA contain motifs to which transcription factors may bind. Prokaryotic gene expression requires a stretch of regulatory DNA called a promoter, which contains two promoter motifs called -10 and -35 boxes. However, these motifs may occur in both promoters and non-regulatory DNA in multiple copies. It is possible that these motifs influence both the evolution and emergence of regulatory DNA, but this has never been thoroughly tested. To understand whether and how promoter motifs influence promoter emergence and evolution, we start from 25 DNA sequences enriched with -10 and -35 box motifs (promoter islands), mutagenize the sequences, and measure gene expression driven by 240'000 mutants. We find that the probability that mutations create an active promoter varies more than 200-fold, but is not correlated with the number of promoter motifs. In most mutants (~67%), the weakening, strengthening, or emergence of a promoter is caused by mutations that modify already existing motifs. Notably, creating new motifs can either increase or decrease promoter activity. Our work demonstrates how promoter motifs influence promoter emergence and evolution. It has implications for predicting and understanding regulatory evolution, de-novo genes, and phenotypic evolution.

AUTHOR CONTRIBUTIONS

TF and AW conceived the study and designed experiments. YS and TF carried out experiments. TF and YS analyzed the data. TF wrote the scripts for computational analysis. TF generated the figures. TF and AW wrote the paper.

CONFLICTS OF INTEREST

The authors declare no competing interests.

INTRODUCTION

Gene regulation is critical to the development and homeostasis of living beings (***Prud'homme et al., 2007***). It is controlled by DNA sequences that encode motifs for transcription factors (TFs) to bind and either activate or repress transcription (***Jacob and Monod, 1961; Seshasayee et al., 2011***). Mutations to these motifs can modulate gene expression, leading to the evolution of new phenotypes ***(Fuqua et al., 2020; Prud'homme et al., 2007)***. Mutations can also create new regulatory sequences from non-regulatory DNA, a process called *regulatory emergence* ***(Rebeiz et al., 2011; Villar et al., 2015)***.

We define a *motif* as a DNA sequence computationally predicted to be compatible with TF binding. We specifically distinguish between a motif and a binding site, because binding sites refer to the location of where a TF binds in the genome, rather than a DNA sequence, and

[1] Department of Evolutionary Biology and Environmental Studies, University of Zurich, Zurich, Switzerland.
[2] Swiss Institute of Bioinformatics, Quartier Sorge-Batiment Genopode, Lausanne, Switzerland.
[3] The Sante Fe Institute, Sante Fe, NM, USA.
* Corresponding email: andreas.wagner "at" ieu.uzh.ch

correspond to only a fraction of all motif locations in a genome *(Avsec et al., 2021; Inukai et al., 2017; Krieger et al., 2022)*.

Although it is commonly thought that regulatory motifs influence both regulatory emergence and evolution, pertinent empirical evidence is sparse and conflicting. On the one hand, such evidence shows that motifs can facilitate promoter emergence and evolution. For example, recent experiments showed that a randomly synthesized DNA with a single motif for a particular TF favored the emergence of tissue-specific gene expression for that TF *(Galupa et al., 2023)*. Likewise, transposable elements contain motifs compatible with the binding of particular TFs *(Lynch et al., 2015; Villanueva-Cañas et al., 2019)*, and these motifs have biased gene regulatory networks towards utilizing these TFs in evolution *(Lynch et al., 2015)*.

On the other hand, there is also evidence that regulatory motifs can impede promoter emergence and evolution. One reason for this is that different regulatory proteins can compete in their binding to shared motifs *(Chauhan et al., 2022; Lagator et al., 2022)*. Another reason is that gene expression can be silenced when regulatory DNA contains multiple motifs for the same TF *(Berman et al., 2002; Bykov et al., 2020; Loell et al., 2024; Perales et al., 2016)*. For example, in mice, retinal "silencers" contains clusters of motifs for the TF CRX, while retinal "enhancers" contain a mixture of CRX and other TF motifs *(Loell et al., 2024)*. A third reason is that clusters of motifs for RNA polymerase binding can cause collisions between RNA polymerase molecules, leading to premature termination of transcription *(Crampton et al., 2006; Hobson et al., 2012; Wang et al., 2023).*

In prokaryotes the primary regulatory sequences are called promoters *(Huerta and Collado-Vides, 2003; van Hijum et al., 2009)*. The canonical promoter recruits the RNA polymerase subunit, σ70 *(Burgess et al., 1969; Huerta and Collado-Vides, 2003; Paget and Helmann, 2003)*, to transcribe target genes. These promoters consists of two *promoter motifs* called the -10 box and the -35 box *(Huerta and Collado-Vides, 2003; Pribnow, 1975; Urtecho et al., 2019)* whose sequences are very well characterized (consensus: `TATAAT` and `TTGAAA`, respectively) *(Burr et al., 2000; Estrem et al., 1998; Ireland et al., 2020; Kinney et al., 2010; Urtecho et al., 2023, 2019; Warman et al., 2021).* We also know how the DNA sequences of promoter motifs, as well as their distances (consensus 17±1 bp) influence gene expression *(Huerta and Collado-Vides, 2003; Klein et al., 2021; Lagator et al., 2022; Mitchell et al., 2003; Tierrafría et al., 2022; Urtecho et al., 2019).* Like in humans *(Gotea et al., 2010)* and invertebrates *(Lifanov et al., 2003)*, most prokaryotic promoters contain multiple regulatory motifs *(Huerta and Collado-Vides, 2003)*, and have multiple transcription start sites *(Mendoza-Vargas et al., 2009)*. It is not clear whether these additional motifs influence promoter activity. If so, it may help to explain why it is difficult to predict promoter strength and activity *(Lagator et al., 2022; Urtecho et al., 2023).*

Recent work shows that promoters can emerge from promoter motifs or adjacent to them *(Fuqua and Wagner, 2023).* However, encoding -10 and -35 box motifs is insufficient to drive transcription. For instance, the *E. coli* genome contains clusters of -10 and -35 box motifs with little or no promoter activity. Such clusters are called *promoter islands* *(Bykov et al., 2020; Panyukov and Ozoline, 2013; Purtov et al., 2014; Shavkunov et al., 2009)*. One study found that promoter activity can either emerge from a promoter island when a -35 box motif is mutated to match the consensus sequence, or counterintuitively, when -10 and -35 box motifs are destroyed *(Bykov et al., 2020)*.

Thus, it is neither understood how additional promoter motifs influence promoter activity, nor is it clear when a promoter motif will facilitate or impede de-novo promoter emergence.

Here, we systematically study the ability of -10 and -35 box motifs to influence the evolution and emergence of promoters. To this end, we select 25 fragments from 25 promoter island sequences, with both regulatory and non-regulatory activity, and screen more than 240'000 mutant variants for promoter activity. We find that ~67% of all promoter activity originates from -10 and -35 box motifs, but the likelihood of mutations creating new promoters does not correlate with the number of motifs. Additionally, mutations can create additional -10 and -35 box motifs to either increase or decrease promoter expression. These results highlight the complex interplay of promoter motifs throughout regulatory evolution and the emergence of new phenotypes.

RESULTS

Parent sequences are enriched with motifs for -10 and -35 boxes.

Promoter islands are ~1kbps (kilo base pairs) long *(Bykov et al., 2020; Panyukov and Ozoline, 2013; Purtov et al., 2014; Shavkunov et al., 2009)*, but for adequate mutational coverage, it is better to work with shorter sequences. We thus identified within 25 promoter islands, a region of 150 bp that showed the highest density of predicted -10 and -35 box motifs for further analysis (**Fig 1A**). To this end, we used position-weight matrices (PWMs) – computational tools to identify promoter motifs (Methods) *(Hertz and Stormo, 1999)*. We refer to these 25 sequences as *parent sequences* (P1-25). On average, each parent contains ~4.22 -10 box motifs and ~5.14 -35 box motifs on each of its two DNA strands (**Fig S1**).

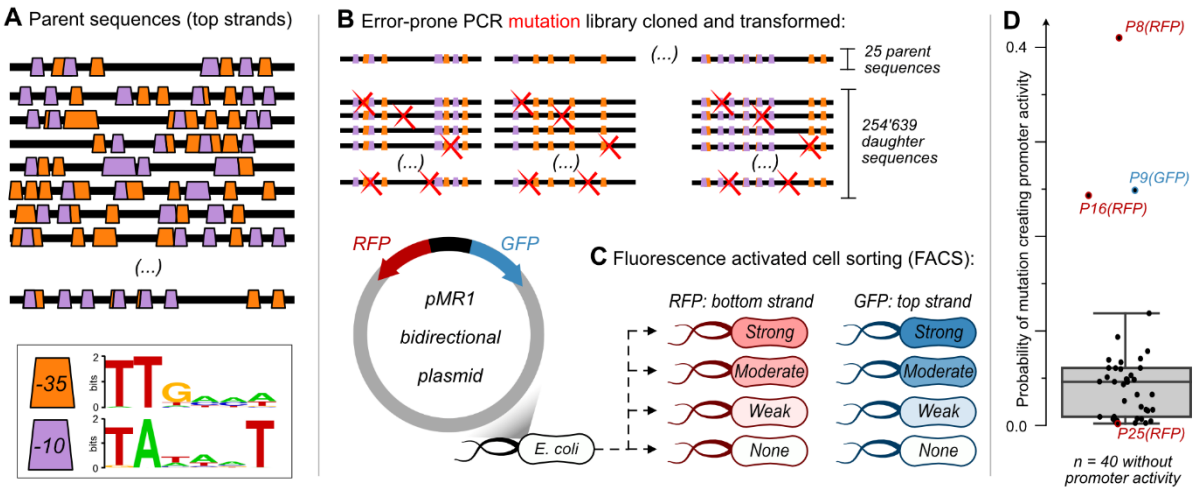

Figure 1. Mutating parent sequences reveals vastly different probabilities of promoter emergence. (A) The location of -10 and -35 boxes in a subset of the parent sequences. See **Fig S1** for the complete set (n=25). Orange trapezoids correspond to -35 box motifs, and magenta trapezoids to -10 box motifs, each identified using position-weight matrices (see sequence logos below and **Fig S1)**. **(B-C)** The Sort-Seq protocol. **(B)** Top: we amplified 25 150bp parent sequences from 25 promoter islands in the *E. coli* genome using an error-prone polymerase chain reaction, generating a mutagenesis library of 245'639 unique daughter sequences. Bottom: we cloned the library into the pMR1 reporter plasmid between a green fluorescent protein (GFP) coding sequence on the top strand (blue arrow) and a red fluorescent protein (RFP) coding sequence on the bottom strand (red arrow). We transformed the plasmid library into *E. coli.* **(C)** Using fluorescence-activated cell sorting (FACS), we sorted the transformed *E. coli* cells into 8 fluorescence bins: none, weak, moderate, and strong, for both RFP and GFP expression (see **Fig S2** for bins). We sequenced the plasmid inserts of cells from each bin, assigning a fluorescence score from 1.0-4.0 arbitrary units (a.u.), ranging from no fluorescence (1.0 a.u.) to strong fluorescence (4.0 a.u.) (see **Fig S4** for score distributions). **(D)** Circles show the probability that mutation creates an active promoter from an inactive parent. Data is shown for each of 40 inactive parents and orientations (i.e., 25 parents ×2 orientations = 50. 50 – 3 top strand promoters – 7 bottom strand promoters = 40.) The height of the box represents the interquartile range (IQR) and the center line the median. Whiskers correspond to 1.5×IQR.

127 **Inactive promoters vary widely in their potential to become active promoters.**
128 Next we created a mutant library of *daughter* sequences from the 25 parent sequences using
129 an error-prone polymerase chain reaction (**Fig 1B**), and measured the extent to which these
130 daughter sequences can drive gene expression using the well-established sort-seq procedure
131 *(Kinney et al., 2010; Peterman and Levine, 2016)*. Specifically, we cloned the library into a
132 bidirectional fluorescence reporter plasmid (pMR1) to measure promoter activity on both DNA
133 strands (top: GFP, bottom: RFP) *(Westmann et al., 2018)*. We then transformed the plasmid
134 library into *E. coli* (DH5α, Takara Japan), sorted the bacteria using fluorescence activated cell
135 sorting (FACS) into eight fluorescence bins (none, weak, moderate, and strong fluorescence,
136 for both GFP and RFP) (**Fig 1C**, see also **Fig S2**), and sequenced the inserts from the sorted
137 fluorescence bins (see methods).

138 Our library comprised 245'639 unique daughter sequences, with an average of 4'913 daughter
139 sequences per parent and orientation (top/bottom) and ~2.5-point mutations per daughter (**Fig**
140 **S2**). Each parent has 3×150 mutational neighbors that differ by a single mutation. We define
141 coverage as the percentage of these 450 bases and positions that are present in at least one
142 daughter sequence for each parent. (Daughters contain 1-10 point mutations.) The mean
143 coverage was 93% (minimum: 80%; maximum: 100%) (**Fig S3**). The mutation library therefore
144 encompasses the majority of neighboring mutations for the 25 parents.

145 We next quantified how strongly each daughter sequence could drive gene expression from
146 the top and bottom strand by calculating a fluorescence score for both GFP and RFP
147 expression, respectively. These scores are bounded between a lowest score of 1.0 arbitrary
148 units (a.u.), indicating no expression, and a highest score of 4.0 a.u., indicating maximal
149 expression (methods). We declared a daughter sequence to have an *active promoter* if its
150 score exceeded 1.5 a.u., as this score lies at the boundary between no fluorescence and weak
151 fluorescence based on the sort-seq bins (methods).

152 Some sequences in our library are unmutated parent sequences, which allowed us to
153 determine that 8/25 of the parent sequences already encode active promoters before
154 mutagenesis. Specifically, one parent drove expression on the top strand (P22), five did on
155 the bottom strand (P6, P12, P13, P18, P21), and two drove expression on both strands (P19
156 and P20). See **Fig S4** for fluorescence score distributions for each parent and its daughters,
157 and **Data S2** for all daughter sequence fluorescence scores.

158 We refer to the remaining 40 parent sequences and orientations as inactive. Although mutating
159 each of the 40 inactive parent sequences could create a promoter, the likelihood P_{new} that a
160 mutation creates an active promoter varies dramatically among parents. For each inactive
161 parent and orientation, **Fig 1D** shows the percentage of active daughter sequences. The
162 median P_{new} is 0.046 (std. ± 0.078), meaning that ~4.6% of all mutants have promoter activity.
163 The lowest P_{new} is 0.002 (P25) and the highest 0.41 (PI7), a 205-fold difference.

164 These P_{new} values do not significantly correlate with the number of daughter sequences, the
165 GC-contents of the parents, and – most notably – with the number of -10 or -35 box motifs
166 (least squares linear regression, p=0.529, 0.930, 0.852, 0.834 respectively) (**Fig S5**). Thus,
167 the number of promoter motifs does not directly influence the likelihood of promoter
168 emergence.

169 **Promoters primarily emerge and evolve from specific subsets of -10 and -35 box motifs.**
170 Next we asked where both active and new promoters are located within the parent sequences.
171 To this end, we first calculated for each parent and its respective daughters, the mutual
172 information $I_i(b, f)$ between the nucleotide identity at each position i and the corresponding
173 fluorescence level f (**Fig 2A**). The essence of this calculation is to determine for every position

i, the probability $p_i(b)$ of that position being an A,T,C, or G and the probability of each sequence having a (rounded) fluorescence score of 1,2,3, or 4 a.u. $p(f)$. Representing these probabilities as circles in a Venn-diagram, the overlap between the circles is the joint probability $p_i(b,f)$ that position i has a specific base b AND a particular fluorescence score f. The larger this joint probability is compared to the individual probabilities, the more important the nucleotide identity at position i is for fluorescence, i.e., for promoter activity. This calculation can reveal positions where RNA polymerase and transcription factors bind ***(Belliveau et al., 2018; Ireland et al., 2020; Kinney et al., 2010)***, as well as DNA regions where promoters most readily emerge (***Fuqua and Wagner, 2023***). The calculation effectively converts all 245'639 data points into maps that reveal where active promoters either already exist or emerge in each of the parent sequences (see methods).

We identified 'hotspots' – regions of especially high mutual information – for each parent sequence ***(Fuqua and Wagner, 2023)*** (see methods). For example, two such hotspots exist in parent P19, which is an active promoter that drives expression from both DNA strands (**Fig 2B**). One hotspot overlaps with a -35 box motif and the other overlaps with a -10 box motif. These hotspots indicate that fluorescence changes when these DNA sequences mutate. Because these sequences additionally match a canonical promoter, they are the likely cause of the promoter activity in P19. Additionally, the number of hotspots that a sequence encodes also correlates modestly with the probability P_{new} (least squares linear regression, $p=1.35\times10^{-4}$, $r^2 = 0.322$) (**Fig S5**). In other words, the more hotspots a parent has, the more likely it is that mutations create a new promoter from it.

Across all 25 parent sequences and for both expression directions (top and bottom strand), we identified a total of 68 hotspots **(Fig 2C**). 29 hotspots occur in the parent sequences with promoter activity. They correspond to locations where mutations either increase or decrease promoter activity. ~17% (5/29) of these hotspots overlap exclusively with -10 box motifs, ~28% (8/29) with -35 box motifs, and ~21% (6/29) overlap with both -10 and -35 box motifs. The remaining ~34% of hotspots overlap with neither a -10 nor a -35 box motif (10/29).

The remaining 39 hotspots occur in inactive parent sequences. Mutations in these locations solely increase fluorescence. Of these 39 hotspots, ~23% (9/39) overlap with -10 box motifs, ~31% (12/39) with -35 box motifs, ~13% with both a -10 and -35 box motifs (5/39), and ~33% with neither motif (13/39) (**Fig 2C-E**). See **Fig S6** for the mutual information plots for all parent sequences and **Data S3** for a table with the hotspots and their coordinates.

Despite this extensive overlap between promoter motifs and hotspots, each parent contains additional -10 and -35 box motifs that do not overlap with hotspots. Of the 211 -10 box motifs, only 25 (~12%) overlap with a hotspot. Similarly, of the 257 -35 box motifs, only 31 (~12%) overlap with a hotspot. For example, the inactive parent P3 contains five -10 box motifs, but only one overlaps with a hotspot (**Fig 2D**). Similarly, the inactive P18 contains seven -10 and -35 box motifs each, but promoters only emerge in three hotspots (**Fig 2E**). In sum, the majority (~67%) of new promoters evolve and emerge from motifs for -10 and -35 boxes, but the presence of a motif does not indicate that promoter activity can emerge or is encoded within the motif.

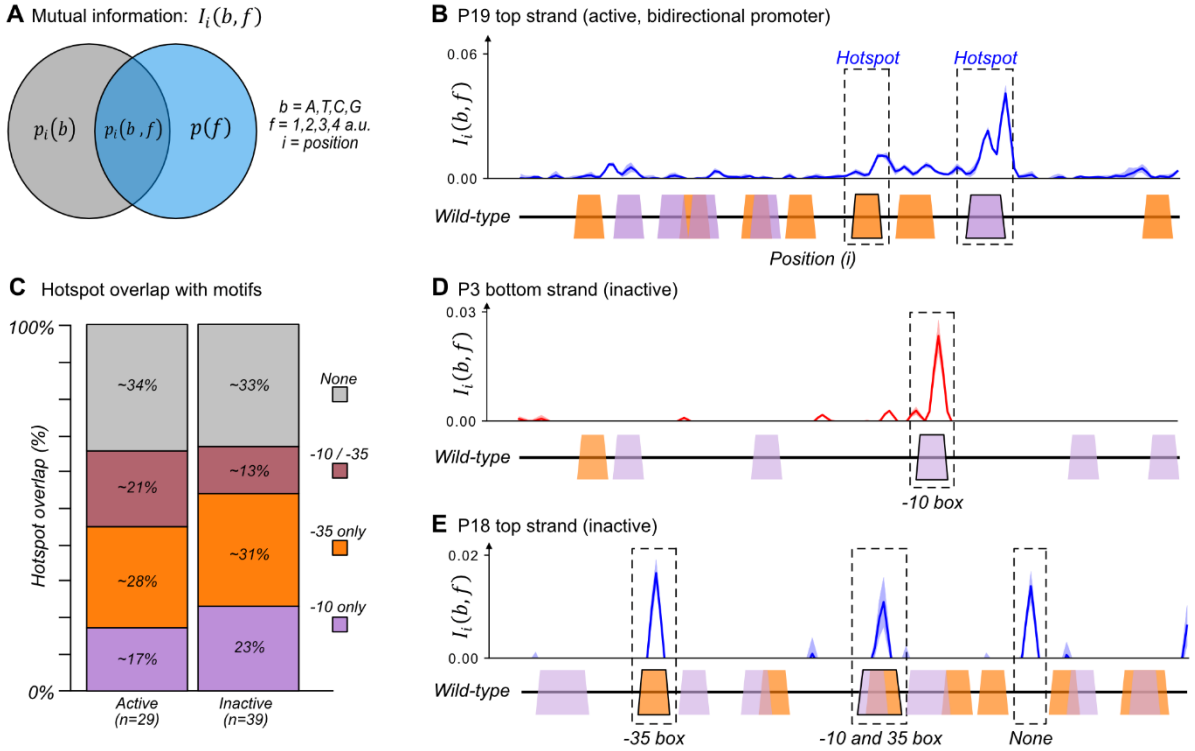

Figure 2. The majority of promoters emerge and evolve within a subset of preexisting promoter motifs. (A) We calculated the mutual information $I_i(b,f)$ between nucleotide identity (b = A,T,C,G) and fluorescence scores rounded to the nearest whole number (f= *1,2,3,4 a.u.*) for each position i in a parent sequence. In essence, the calculation compares the probability $p_i(b)$ of a base b occurring at position i , and the probability $p(f)$ that a sequence has a fluorescence score f. The joint probability $p_i(b,f)$ is the probability that a sequence with base b at position i has fluorescence score f. The greater the joint probability is compared to the individual probabilities, the more important the base at this position is for promoter activity. See methods. **(B)** An example of how to interpret mutual information using position-weight matrix (PWM) scores of predicted -10 and -35 box motifs. Top: we plot the mutual information $I_i(b,f)$ for P19's top strand. P19 is an active promoter on both DNA strands. Solid line: mean mutual information. Shaded region: ± 1 standard deviation when the dataset is randomly split into three equally sized subsets (methods). Bottom: position-weight matrix (PWM) predictions for the -10 box motifs (magenta trapezoids) and -35 box motifs (orange trapezoids) along the wild-type parent sequence. We define hotspots as mutual information peaks greater than or equal to the 90th percentile of total mutual information (methods), and highlight them with dashed rectangles. **(C)** Stacked bar plots depicting the percentage of hotspots overlapping with -10 box motifs only (magenta), -35 box motifs only (orange), both -10 and -35 box motifs (red), or with neither (gray). We plot this both for active parents (left) and inactive parents (right). **(D)** Analogous to (B) but for the bottom strand of P3. P3 is an inactive parent sequence. Hotspot overlaps with a -10 box motif. **(E)** Analogous to (B) but for the top strand of P18. P18 is an inactive parent sequence. Hotspots overlap with (from left to right) a -35 box motif, both a -10 and a -35 box motif, and neither (None). **Fig S6** shows analogous mutual information plots for daughters derived from each parent sequence.

Promoters can emerge when mutations create motifs but not by destroying them.

We hypothesized that promoters emerge when mutations create -10 and -35 box motifs. To test this hypothesis, we examined each hotspot and used PWMs to find out whether a subset of the daughter sequences gains a -10 or -35 box motif in the hotspot. We then asked whether gaining a -10 or -35 box motif leads to a significant increase in fluorescence that indicates the creation of a new promoter (Mann-Whitney U-test, **Fig. S7** and methods)

We identified 5 and 4 hotspots in which gaining a -10 box motif or a -35 box motif creates a de-novo promoter by increasing fluorescence by more than +0.5 a.u. (**Fig 3A**). For ~67% (6/9) of these hotspots, the locations of the newly created -10 and -35 box motifs overlap with preexisting -10 and -35 box motifs.

As examples, we highlight two hotspots involving the creation of a -10 box. Parent P16 gains promoter activity when mutations create a -10 box downstream of a preexisting -35 box motif (**Fig 3B**), increasing median fluorescence by +1.99 a.u. (**Fig 3C**) (two-tailed MWU test, $q=7.64\times10^{-32}$). We call the act of mutations creating a -10 box downstream of a preexisting -35 box motif *Shiko emergence* (*Fuqua and Wagner, 2023*). The term is a homage to the Sumo exercise Shiko, where the wrestler firmly plants their foot firmly on the floor, and lowers their other foot to a firm position. In contrast, parent P9 gains promoter activity when mutation creates a new -10 box that does not lie downstream of an existing -35 box motif (**Fig 3D,E,** median fluorescence gain +1.8 a.u., two-tailed MWU test, $q=2.83\times10^{-173}$). See **Fig S8** for the other hotspots in which -10 boxes are created.

We also highlight one hotspot where gaining a -35 box creates de-novo promoter activity. Specifically, parent P1 gains promoter activity when mutations create a -35 box upstream of a preexisting -10 box motif **(Fig 3F**), which increases fluorescence by +0.74 a.u. (**Fig 3G**, two-tailed MWU test, $q=4.25\text{x}10^{-42}$). This is also an example of Shiko Emergence (Shiko -35). See **Fig S8** for the other hotspots in which -35 boxes are created. We did not find any hotspots where a -35 box is created without a downstream -10 box motif.

Prompted by an earlier report *(Bykov et al., 2020)*, we also asked whether mutations that destroy -10 or -35 box motifs can increase promoter activity. No such mutations exist in our data (see **Fig 3A**).

To summarize, we found 9 hotspots where mutations created -10 and -35 boxes that lead to de-novo promoter emergence. When -10 boxes are gained, the majority (three of five) form downstream of a preexisting -35 box motif (Shiko -10 emergence). The remaining two -10 boxes do not form near a -35 box motif (gain -10, **Fig 3H**). Four of the four newly formed -35 boxes form upstream of a -10 box motif (Shiko -35). We did not find any hotspots where creating a -35 box without a downstream -10 box motif leads to promoter emergence. In the majority of the 9 hotspots (6 of 9), new -10 or -35 boxes overlap preexisting -10 and -35 box motifs.

Gaining boxes can increase or decrease promoter activity (by more than one mechanism)

We next asked how gaining and losing -10 and -35 box motifs can change expression driven by active parent sequences. To this end, we repeated the previous analysis but for the active parents.

We first identified 5 and 3 hotspots in which losing a -10 box motif or -35 box motif *decreases* expression (**Fig S9A**). These particular hotspots revealed where promoters are located in each parent. For example, for parent P12 (**Fig S9**), losing a -35 box decreases fluorescence by -1.57 a.u. (**Fig S9**) (two-tailed MWU test, $q=6.28\times10^{-67}$), and losing a -10 box decreases fluorescence by -1.41 a.u. (two-tailed MWU test, $q=6.28\times10^{-91}$). Based on these data and the close spacing (18 bp) of these two motifs, we can infer that they constitute the binding sites for the promoter in P12 (**Fig 4A**). See **Fig. S9** for additional examples. We did not find any hotspots in which destroying a -10 box motif or a -35 box motif increases expression (see **Fig S9A**).

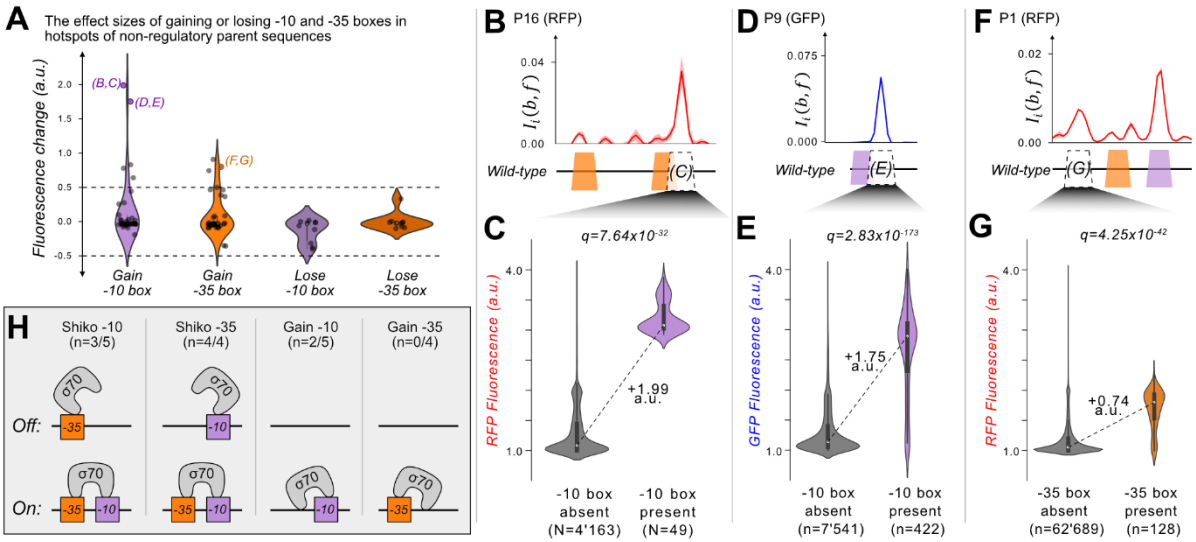

Figure 3. Gaining -10 and -35 boxes that overlap with promoter motifs creates de-novo promoters. (A) The change in fluorescence (arbitrary units, a.u.) when gaining or losing -10 and -35 box motifs in mutual information hotspots of inactive parent sequences (see **Fig S7** for calculation overview). Dotted lines indicate an effect size threshold of ± 0.5 a.u. Each circle corresponds to a gain or loss of a box motif in a mutual information hotspot (see **Fig 2** for hotspots). Circles with letters in parentheses refer to the corresponding figure panels. The volume of each violin plot corresponds to a kernel density estimate of each distribution. **(B)** The bottom strand of parent P16. Top: Mutual information $I_i(b,f)$ between nucleotide identity and fluorescence at each position. Solid red line: mean mutual information, shaded region: ± 1 standard deviation when the dataset is randomly split into three equally sized subsets (methods). Bottom: position-weight matrix (PWM) predictions for the -10 box motifs (magenta trapezoids) and -35 box motifs (orange trapezoids) along the wild-type parent sequence. Dotted trapezoid indicates the region of interest analyzed in the subsequent panel. **(C)** Fluorescence scores (a.u.) for daughter sequences without (left) and with (right) a -10 box motif in the region of interest defined in (B). We tested the null hypothesis that the gain of the motif significantly increases fluorescence (two-tailed Mann-Whitney U [MWU] test). The q-values correspond to Benjamini-Hochberg-corrected p-values (methods) (two-tailed MWU test, $q=7.64\times10^{-32}$). Within the violin plot is a box plot, where the box represents the interquartile range (IQR) and the white circle the median. Whiskers correspond to 1.5×IQR. **(D)** Analogous to (B) but for the top strand of parent P9. **(E)** Analogous to (C) except for the region of interest defined in (D) (two-tailed MWU test, $q=2.83\times10^{-173}$). **(F)** Analogous to (B) but for the bottom strand of parent P1. **(G)** Analogous to (C) except for gaining a -35 box instead of a -10 box in the region of interest defined in (F) (two-tailed MWU test, $q=4.25\times10^{-42}$). **(H)** Promoter emergence models from left to right. Promoters emerge by gaining -10 boxes downstream of preexisting -35 box motifs (Shiko -10), gaining -35 boxes upstream of preexisting -10 box motifs (Shiko -35), gaining a -10 box independent of an upstream -35 box motif, or gaining a -35 box upstream independent of a preexisting -10 box motif. See **Fig S8** for additional examples.

We also found 4 and 1 hotspot(s) in which gaining a -10 or -35 box further increases expression. More surprisingly, in 4 and 6 hotspots gaining a -10 or -35 box *decreases* expression (n= 4+1+4+6, 15 hotspots with increased or decreased expression) (see **Fig S9A**). To understand how this is possible, we analyzed each parent sequence where this occurs in detail. This analysis allowed us to group such events into three categories. That is, mutation can 1) create a *tandem motif* that lowers expression, 2) shift -10 and -35 boxes to modulate expression, or 3) create additional -10 and -35 box motifs that destroy the original promoters and lower expression (**Fig 4**). Next we briefly describe examples of each category.

For 2 of the 15 hotspots (~13%), mutations create a *tandem motif,* where two -10 or -35 box motifs occur in head-to-tail orientation. For example, when mutations of the aforementioned parent sequence P12 create a -35 box motif upstream of the existing -35 box, median fluorescence decreases by 1.1 a.u. (two-tailed MWU test, $q=3.35\times10^{-5}$) (**Fig 4B**). Similarly, when mutations in P12 create a -10 box motif upstream of the mapped -10 box, median fluorescence also decreases by 0.61 a.u. (two-tailed MWU test, $q=4.36\times10^{-4}$) (**Fig 4C**).

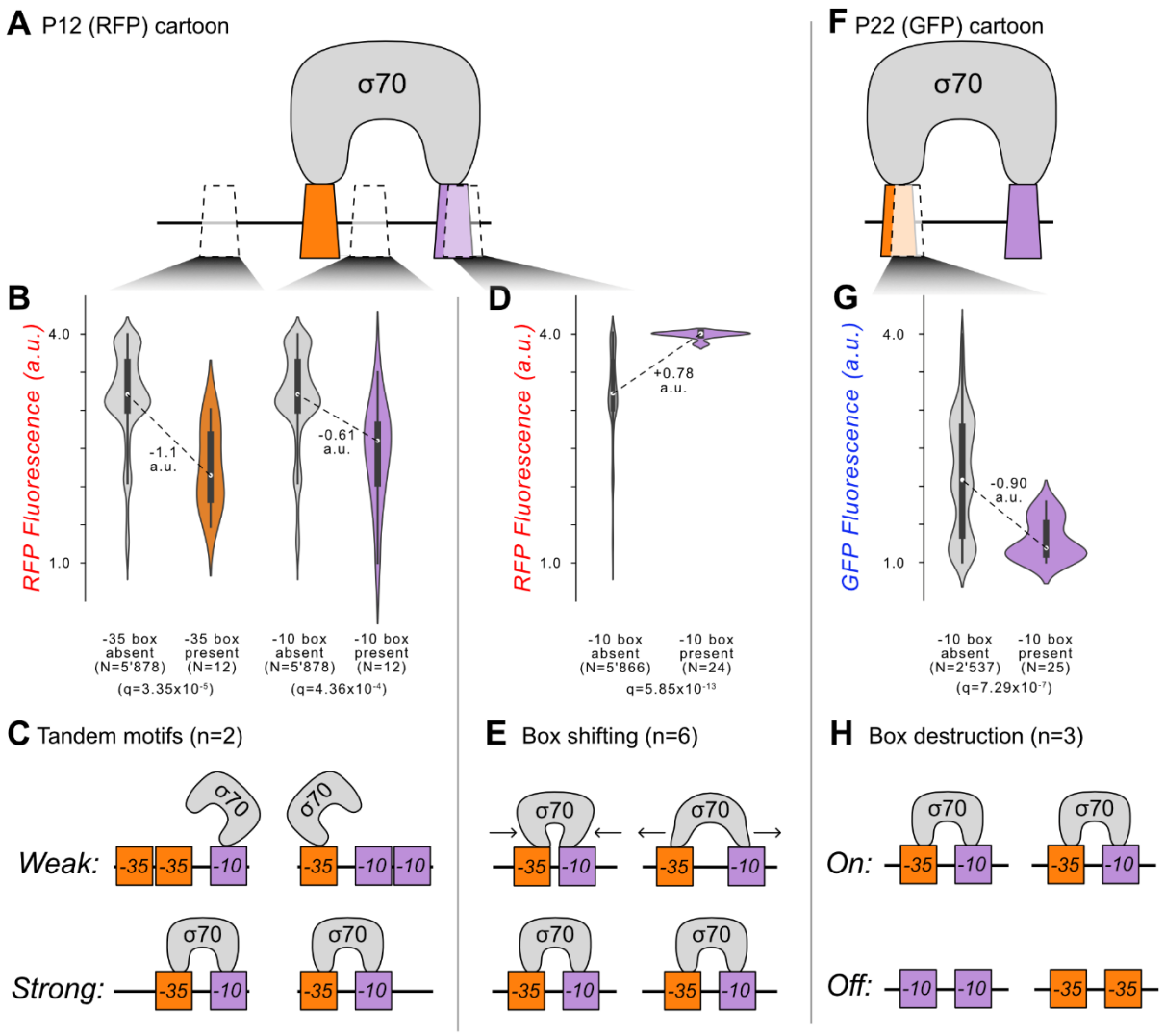

Figure 4. Gaining -10 and -35 boxes modulates promoter activity. (A) A cartoon for the promoter mapped on the bottom strand of P12 based on data from **Fig S9.** Orange trapezoids = -35 boxes, magenta trapezoids = -10 boxes, dashed trapezoids = regions of interest in subsequent figure panels. **(B)** We test the null hypothesis that the fluorescence scores in each group have the same central tendency using a two-sided Mann-Whitney U (MWU) test. We test this null hypothesis for daughter sequences with vs without a -35 box motif (left comparison) or with vs without a -10 box motif (right comparison) using a Mann-Whitney U (MWU) test. The q-values correspond to Benjamini-Hochberg-corrected p-values (methods; (two-tailed MWU test, $q=3.35\times10^{-5}$ and $q=4.36\times10^{-4}$, respectively). The areas of the violin plots are the kernel density estimates (KDE) of each distribution. Within each violin plot is a box plot, where the box represents the interquartile range (IQR) and the white circle the median. Whiskers correspond to 1.5×IQR. Dotted lines bridging the box plots with numbers underneath correspond to the median change in fluorescence (a.u.). **(C)** A proposed mechanism whereby gaining -35 boxes adjacent to -35 boxes or -10 boxes adjacent to -10 boxes lowers expression. **(D)** Analogous to (B) but for the presence or absence of a -10 box shifted +1 bp downstream from the modeled -10 box (two-tailed MWU test, $q=5.85\times10^{-13}$). **E)** A proposed mechanism where mutations shift -10 and -35 boxes either closer or further apart to modulate promoter strength. See **Fig S10** for 5 additional examples. **(F)** Analogous to (A) but for the promoter mapped on the top strand of P20. **(G)** Analogous to (B) but for the presence or absence of a -10 box motif overlapping with the modeled -35 box (two-tailed MWU test, q=7.29×10-7). **(H)** A proposed mechanism whereby mutations create new -10 or -35 box motifs in the locations of existing promoter binding sites, destroying the promoter. See **Fig S10** for two additional examples.

For 6 of the 15 hotspots (40%), mutations shift the location of -10 and -35 boxes. For example, mutations can shift the -10 box of parent P12 +1 bp away from the -35 box, which increases median expression by +0.78 a.u. (**Fig 4D**) (two-tailed MWU test, $q=5.85\times10^{-13}$). See **Fig S10** for additional hotspots where such shifting occurs (**Fig 4E**).

For 3 of the 15 hotspots (20%), we find that mutations can create -10 or -35 box motifs overlapping -10 and -35 boxes from the putative promoters we mapped in **Figure S9**. For example, for parent P22, where our mutational data had allowed us to map the active -35 and -10 boxes (**Fig 4F**), mutations can change the -35 box into a -10 box motif, which decreases expression by 0.90 a.u. (**Fig 4G**) (two-tailed MWU test, $q=7.29\times10^{-7}$). Thus, while the loss in expression appears to be caused by a gain of a motif, this gain also entails of a loss of an existing, active box (**Fig 4H**). See **Fig S10** for additional examples.

The remaining 4 of 15 hotspots (~27%) are located in P20 (**Fig. S11**), which encodes a bidirectional promoter. However, because our mutational data did not allow us to confidently map this promoter on either strand of P20, we cannot resolve why gaining -10 or -35 box motifs may increase expression (in 2 of the 4 P20 hotspots) or decrease expression (in the remaining 2 hotspots, **Fig. S11**) of this parent sequence.

DISCUSSION

We found that sequences enriched with -10 and -35 box motifs without promoter activity vary dramatically (more than 200-fold) in the probability P_{new} that mutations create active promoters in them (P_{new} = 0.002 to 0.41, see **Fig 1D**). When trying to understand the reasons for this variation, we found that P_{new} is not significantly correlated with the number of existing -10 or -35 box motifs (least squares linear regression, p=0.852, 0.834 respectively). In addition, hotspots of promoter emergence coincide with only ~12% of the -10 and -35 box motifs. However, P_{new} correlates with the number of mutual information hotspots (least squares linear regression, $p=1.35\times10^{-4}$, $r^2 = 0.322$, see **Fig S5**). For instance, three parental sequences with high P_{new} (P8, P9, and P16, see **Fig 1D**) encode multiple hotspots (3,3, and 5 hotspots respectively, see **Fig S6**). In each of these hotspots, promoters emerge when mutations create new -10 and -35 boxes (see **Fig 3** and **Fig S8**). Sequences with the lowest emergence probability, such as the bottom strand of P25, contain no hotspots (**Fig S6**). Therefore, promoter emergence is best explained by how readily mutations create *additional* promoter motifs, not by the number of preexisting -10 and -35 box motifs. Additionally, ~78% (7/9 hotspots) of emergence hotspots, gain new -10 and -35 boxes adjacent to corresponding -10 and -35 box motifs (Shiko Emergence, see **Fig 3H**), suggesting that the location of new and preexisting motifs also influences promoter emergence.

-10 and -35 box motifs, however, influence where promoters emerge. We found that the majority (~67%) of all mutual information hotspots overlap with -10 or -35 box motifs (see **Fig 2C**). This can partially be explained by our finding that mutations create additional -10 and -35 boxes upstream or downstream of -35 and -10 box motifs respectively, to build promoters (see **Fig 3**). Additionally, mutations within the promoter motifs can shift their locations, change a -35 box into a -10 box motif, or vice versa (see **Fig 3** and **Fig S8**). This finding may help to explain why a previous study concluded that destroying promoter motifs creates promoter activity ***(Bykov et al., 2020).*** Specifically, destroying a -10 or -35 box motif can create a de-novo promoter, but only if this destruction simultaneously creates a new -10 or -35 box (see **Fig 3A**).

When asking how mutations change the activity of already active parent sequences, we found that their ability to shift the locations of -10 and -35 boxes is especially important. For example,

in 6 hotspots, mutations that shift -10 and -35 boxes either increase or decrease expression (see **Fig 4E**). This shifting also explains why ~67% of hotspots in active sequences overlap with existing -10 and -35 box motifs. This finding is consistent with previous studies, which demonstrate that the distance between -10 and -35 boxes is an integral component of promoter strength, and that deviations from the 17±1 bp spacing can result in lower expression *(Klein et al., 2021; Lagator et al., 2022; Urtecho et al., 2019).*

Promoter activity can be further modulated by the creation of tandem motifs in parent P12. Such tandem motifs do not abolish gene expression but decrease it by about one half (**Fig 4B** and **Fig 4C**). One possible explanation for this halving is that RNA polymerase can bind to both parts of the tandem motif (i.e. both -10 boxes or both -35 boxes), but only binding to one of these two yields promoter activity. To understand the biophysical mechanism behind this phenomenon is a task for future work. Regardless of this mechanism, the observation underlines that DNA sequences flanking a promoter can be important for protein binding *(Mitchell et al., 2003),* as has also been observed in eukaryotic transcriptional regulation *(Afek et al., 2014; Chiu et al., 2022; Farley et al., 2015; Gordân et al., 2013)*. Collectively, the shifting of -10 and -35 boxes, and the creation of tandem motifs demonstrate how mutations can readily create promoters with a wide dynamic range of activity. This ability facilitates natural selection's fine-tuning of a promoter to precise expression levels, within a small sequence search space that is easily accessible by few DNA mutations.

Overall, our study demonstrates that mutations to -10 and -35 box motifs are the primary paths to create new promoters and to modulate the activity of existing promoters. On the one hand, this is exciting for studying de-novo genes and the evolution of novel gene expression, because it suggests that promoter emergence and evolution may be predictable *(Lässig et al., 2017; Stern and Orgogozo, 2008)*. On the other hand, our observation that promoter motifs influence where new regulatory sequences can emerge, leads to many exciting insights about regulatory emergence throughout the genome, plasmids, and transposable elements.

For instance, new enhancer sequences in eukaryotes primarily emerged from specific families of transposable elements *(Villar et al., 2015; Yue et al., 2014)*. Furthermore, transposons encoding particular motifs influence which TFs are utilized in a gene regulatory network *(Lynch et al., 2015)*. Collectively, observations like these suggest that the identity of a DNA sequence heavily influences how gene regulation emerges and evolves, and thereby which novel phenotypes are most likely to arise by chance.

DATA AVAILABILITY

Data S1 is a list of the DNA sequences for the primers and promoter island parent sequences in this study. Data stored as an Excel spreadsheet.

Data S2 is a dataframe with all of the daughter sequences and their respective fluorescence scores after cleaning the dataset. Data stored as a csv file.

Data S3 is a dataframe with each identified hotspot and whether it overlaps with a -10 or -35 box. Data stored as a csv file.

Data S4 is a dataframe with the output from the gain-loss analysis for both the top and bottom strand. Data stored as a csv file.

Data S5 is an Excel spreadsheet to rapidly reproduce the main figures (to the best of Excel's capabilities).

A Jupyter notebook with all of the python scripts to recreate the analysis and figures in this study, as well as Data S1-S5 are available at the Github repository: https://github.com/tfuqua95/promoter_islands

The sequence reads are available at the Sequence Read Archive (SRA) with accession number: PRJNA1071572: https://www.ncbi.nlm.nih.gov/bioproject/1071572

METHODS

Position weight matrices (PWMs)

To create PWMs for -10 and -35 box motifs, we obtained a list of -10 and -35 box sequences from Regulon DB *(Tierrafría et al., 2022)*, and converted them into PWMs using `Biopython.motifs` from the `Biopython` package *(Cock et al., 2009)* (v1.79). We deliberately assumed a uniform nucleotide composition (25% A, T, C, or G) in this process, because doing so allowed us to test PWM prediction performance in a variety of different sequence backgrounds. For every input sequence, a PWM returns an output score in bits. The higher this score is, the more likely it is that the input sequence can be bound by the protein the PWM represents.

To classify whether an output score is strong enough to be classified as a -10 or -35 box motif, we used the standard practice of setting a threshold equal to the information content of the PWM *(Hertz and Stormo, 1999)*. The -10 box in our study has an information content of 3.98 bits and the -35 box of 3.39 bits. We classified input sequences with scores at least this high as -10 or -35 box motifs, respectively. In **Fig S9** we also plot "low-affinity" -10 and -35 box motifs. For these motifs, we halved the thresholds (1.99 and 1.70 bits, respectively).

Amplifying parent sequences and plasmid MR1 with PCR

We acquired the genomic coordinates for the promoter island sequences from *(Panyukov and Ozoline, 2013)*. We used a polymerase chain (PCR) reaction to amplify 78 parent sequences from the genome, using Q5 polymerase (NEB, USA product #M0491). The reaction amplifies each parent sequence from the genome, and additionally concatenates short sequences to the 5' and 3' ends of the inserts (5'-`GGCTGAATTC`…insert…`GGATCCTTGC`-3'). These overhangs allowed us to carry out the error-prone PCR with a single set of primers. See **Data S1** for the list of primers and **Fig S12** for an overview of the PCR.

To amplify the parent sequences from the genome, we performed each PCR in a 50 uL reaction volume with the following reagents: 1 uL of each primer (2× primers, 2uL total, concentration 100 uMol), 5 uL Q5 reaction buffer, 1 uL 10 mM dNTPs (Thermo Scientific, USA, product #R0191), 1 uL of the genomic DNA extracted using a Wizard Genomic DNA Purification Kit according to the manufacturer's instructions (A1120, Promega USA), 1 uL Q5 high-fidelity DNA polymerase, and 40 uL of water. We carried out the PCR in a thermal cycler (C1000 Touch Thermal Cycler, Bio-Rad, USA) with 30 cycles at 55ºC for annealing and 72ºC for primer extension, both for 30 seconds. To purify the PCR products, we separated them on a 1% agarose gel, excised them, and used a Qiagen QIAquick Gel Purification Kit (Qiagen, Germany, product #28706) following the manufacturer's instructions. To verify the purification's success and estimate the final concentrations of each product, we used a Nanodrop One spectrophotometer (Thermo Scientific, USA).

To create the mutagenesis library of parent sequences, we pooled the 78 PCR products such that each product had the same concentration in the pool. We then performed a single error-prone polymerase chain reaction on the pooled products to create a mutagenesis library. To this end, we used GoTaq polymerase (Promega, USA, product #M3001). Specifically, we combined 1 uL of two PCR primers complementary to both the pMR1 plasmid and to the

491 sequences concatenated to the ends of the initial PCR (1 uL forward and 1 uL reverse primer,
492 each at a 100 uMol l^{-1}) (see **Data S1** and **Fig S12**), 10 uL of GoTaq reaction buffer, 1 uL 10
493 mM dNTPs (Thermo Scientific, USA, product #R0191), 1 uL of pooled DNA, and 1 uL of GoTaq
494 polymerase. We added water to a total of 98 uL, then added 2 uL of 15 mMol $MnCl_2$ to the
495 reaction. We then excised and purified the product as described for the parent sequences.

496 We additionally used Q5 polymerase to create and amplify linear copies of pMR1 (see **Data**
497 **S1** for primer sequences and **Fig S12**). We carried out the necessary PCR as described for
498 the parent sequences but for an extension time of 2 minutes and 30 seconds.

499 **Molecular cloning**

500 We cloned the error-prone PCR library into pMR1 at the EcoRI and BamHI sites using
501 NEBuilder (New England Biolabs, USA, product #E2621) as follows: 100 ng of linear pMR1,
502 25 ng insert, 5 uL NEBuilder mastermix, and water to 10 uL total volume. To increase the
503 reaction efficiency, we added 1 uL of T4 DNA ligase buffer (New England Biolabs, USA,
504 product #B0202S). Using a thermal cycler (C1000 Touch Thermal Cycler, Bio-Rad, USA) we
505 incubated each assembly reaction for 1 hour at 50ºC.

506 Subsequently, we electroporated our product directly into *E. coli* DH5α electrocompetent cells
507 (Takara, Japan, product #9027) by adding 2 uL of (unpurified) product to 2× 50 uL aliquots of
508 *E. coli* (100 uL total) in a 2 mm electroporation cuvette (Cell Projects, England, product #EP-
509 202), and electroporated the cells using a Bio-Rad MicroPulser (Bio-Rad, USA). For recovery,
510 we then added 1 mL of Super Optimal Broth with Catabolite Repression Medium (SOC,
511 provided with the electrocompetent cells (Takara, Japan, product #9027), shaking the cells at
512 230 RPM at 37ºC for 1.5 hours (Infors HT, Switzerland, Multitron).

513 We then plated 5 uL of the bacterial culture onto a petri dish containing LB-agar supplemented
514 with 100 ug/ml of chloramphenicol, and incubated the plate at 37ºC overnight. In parallel, we
515 added 9 mL of LB-chloramphenicol (100 ug/mL) to the remaining 995 uL of bacteria (in SOC),
516 and incubated the resulting culture overnight. The following morning, we manually counted
517 colonies on one quarter of the plate, and estimated the total number of clones (cells) in the
518 original electroporated culture by multiplying this value by 4×200.

519 **Sort-seq controls**

520 We synthesized three control promoter sequences (**Data S1)** as fiducial markers for defining
521 the fluorescence sorting gates for sort-seq. The insert DNA sequences were chemically
522 synthesized (Integrated DNA Technologies, USA). We then amplified these promoters, cloned
523 them into plasmid MR1, and transformed *E.coli* with them as described in "Molecular Cloning."
524 The first is the promoter iGem bba_j23110 on the top DNA strand, which drives moderate GFP
525 expression from plasmid pMR1. The second is the reverse complement of this promoter, which
526 drives moderate RFP expression from the bottom DNA strand of pMR1. The third and final
527 (negative) control is the wild-type pMR1 plasmid without any insert in its multiple cloning
528 sequence.

529 **Sort-Seq**

530 To perform sort-seq, we first added 100 uL of the glycerol stock of our mutagenesis library to
531 1 mL of LB-chloramphenicol (100 ug/ml). We then allowed the resulting culture to shake at
532 230 RPM and 37ºC overnight (~16 hours) on an Infors HT (Multitron, Switzerland) shaking
533 incubator. Subsequently, we centrifuged the culture and washed the cell pellet twice with
534 Dulbeco's Phosphate Buffered Saline (PBS) (Sigma, USA, D8537). We then resuspended the
535 pellet in PBS.

536 To detect fluorescence caused by GFP and RFP expression, we measured green fluorescence
537 using a 488 nm laser (FITC-H) at 750 volts, and red fluorescence with a 633 nm laser (PE-H)
538 at 510 volts on an Aria III cell sorter (BD Biosciences, USA). We used the following
539 fluorescence gates for sort-seq (**Figure S2**).

540 RFP bin #1 (none, i.e., no fluorescence): We defined a minimum boundary to not sort cell
541 debris, salts, empty droplets, and other impurities, as the larger of two PE-H values. These
542 values are the minimum PE-H of the negative control (empty pMR1 plasmid) and the minimum
543 PE-H of the opposite fluorophore positive control (GFP in this case). The upper boundary of
544 this bin is the highest PE-H value detected for these same controls.

545 RFP bin #4 (high): We defined the lower boundary of this bin using the mean fluorescence
546 level of the positive RFP control. This bin does not have an upper bound, because it
547 encompasses the highest levels of fluorescence.

548 RFP bins #2 and #3 (low and moderate): the lower bound of bin #2 begins at the upper bound
549 of bin #1. The upper bound of bin #3 ends at the lower bound of bin #4. The upper bound of
550 bin #2, which is identical to the lower bound of bin #3, equals the average of the lower
551 boundary of bin #4 and the upper bound of bin #1.

552 We defined the bins for GFP analogously, but with GFP and RFP controls swapped, with the
553 following exception: Because the GFP positive control produces a bimodal FITC-H distribution,
554 we defined the lower bound of bin #4 for green fluorescence as the peak of the higher mode
555 of this distribution. See **Fig S2** for an illustration of the bins.

556 We sorted the library using two consecutive rounds of sorting on consecutive days. On the
557 first day, we sorted 2'160'000, 71'545, 28'399, and 22'720 cells into GFP bins none, low,
558 moderate, and high, respectively; and 2'160'000, 540'000, 101'636, and 76'898 cells into RFP
559 bins none, low, moderate, and high, respectively. After sorting, we added 1 mL of SOC medium
560 (Sigma, USA, product #CMR002K) to the sorted cultures, incubating the cells at 37ºC and
561 shaking for two hours at 230 RPM (Infors HT, Switzerland, Multitron). Following this recovery
562 period, we added 9 mL of LB-Chloramphenicol (100 ug/ml chloramphenicol) to each culture
563 and incubated them overnight (~16 hours) under the same conditions.

564 On day two, we once again washed the cultures and re-sorted cells in each culture into the
565 same fluorescence bin. That is, we sorted cells from GFP-none into GFP-none, GFP-low into
566 GFP-low, and so forth. This resorting step ensures that each genotype fluoresces within the
567 same boundaries as on the previous day, and reduces the likelihood of propagating sorting
568 errors into subsequent analyses. The resulting number of cells for each bin were as follows:
569 GFP-none: 6'480'000, GFP-low: 216'000, GFP-moderate: 90'000, GFP-high: 69'000, RFP-
570 none: 6'480'000, RFP-low: 540'000, RFP-moderate: 306'000, RFP-high 231'000 cells. We
571 allowed the cells to recover as described at the end of day one.

572 After ~16 hours of overnight culture, we created glycerol stocks for each culture (8 cultures
573 total) as described in "Molecular Cloning." From the remaining culture volume, we isolated the
574 plasmids using a Qiagen QIAprep Spin Miniprep kit (Qiagen, Germany, product #27104) as
575 described by the manufacturer. We amplified the plasmid inserts using PCR as described in
576 "Molecular Cloning", using primers (**Data S1**) that add a unique multiplexing barcode onto the
577 5'-end of each PCR product from each bin. In addition, we isolated the inserts from the
578 unsorted library, and endowed them too with a unique barcode. This procedure yielded 9
579 (=8+1) sequence samples, each with a unique barcode. We then pooled equimolar amounts

of these samples, and sequenced them using Illumina paired-end sequencing (Eurofins GmbH, Germany).

Processing sequencing reads

Using Flash2 (*Magoč and Salzberg, 2011*), we merged the paired-end reads that resulted from Illumina sequencing. Each paired-end read contains palindromic cut-sites for 5'-EcoRI (`GAATTC`) and 3'-BamHI (`GGATCC`). To orient all of the paired-end reads in the same direction, we searched each paired-end read for both cut-sites, discarding any sequence that did not encode both, and took the reverse complement of the read if the BamHI site was upstream of the EcoRI site. We then identified the tagmented barcode sequence upstream of the EcoRI site, classifying from which fluorescence bin the read originated. We then cropped the sequences to remove the barcodes, BamHI, and EcoRI sites, and counted the total number of reads within every bin. We refer to each of these unique paired-end read sequences as *daughter sequences.*

To focus on point mutations rather than insertions and deletions, we removed daughter sequences with a length different from the wild-type 150 bp. To minimize the influence of sequencing errors in our dataset, we removed daughter sequences that did not occur at least once in the unsorted library, and daughter sequences with less than thirty reads in the entire dataset.

To map each daughter sequence to its respective template parent sequence, we calculated the Hamming distance (i.e. the number of nucleotide differences between two sequences) between each daughter sequence and the 78 parent sequences, and identified the parent as the sequence with the smallest Hamming distance. To minimize our likelihood of mapping the daughter sequences to the wrong parent sequence, we removed daughter sequences from the dataset for which the closest Hamming distance was greater than 10. Because the error-prone PCR created different numbers of daughter sequences per parent sequence, we also removed all parent and their respective daughter sequences if there were less than 2'000 unique daughter sequences. After these calculations and filtration steps, our dataset contained 245'639 daughter sequences derived from 25 parent sequences.

To calculate fluorescence scores (F) we used in the next analysis step, we calculated (F) using Equation (1):

$$F = \frac{\sum_{f=1}^{4}(f \times Reads_f)}{\sum_{f=1}^{4}(Reads_f)} \qquad (1)$$

Here, f is an integer index corresponding to each of the four fluorescence bins, i.e., f = 1,2,3,4 corresponds to no fluorescence, low, moderate, and high fluorescence, respectively. $Reads_f$ is the number of times the sequence was identified in each fluorescence bin f. We calculated F for both green and red fluorescence. Each score is in arbitrary units (a.u.) of fluorescence.

See **Data S2** for a csv file with the daughter sequences and their respective fluorescence values, which we analyzed further with the code on the GitHub repository: https://github.com/tfuqua95/promoter_islands.

Mutual information

To calculate mutual information between nucleotides and fluorescence scores, we first randomly split the dataset into three equal-sized pseudo-replicates (r1, r2, and r3) to minimize the effects of sampling biases as well as sorting errors when calculating mutual information. For each pseudo-replicate, we calculated the mutual information $I_i(b, f)$ between the

nucleotide identity b and fluorescence score f score at each position i ($1<i<150$), of every daughter sequence using equation (2), as defined in ref. *(Kinney et al., 2010)*:

$$I_i(b,f) = \sum_b \sum_f p_i(b,f) \log_2 \frac{p_i(b,f)}{p_i(b) \times p(f)} - \frac{(n_b - 1)(n_f - 1) \log_2 e}{2N} + O(N^{-2}) \qquad (2)$$

In the left term on the right-hand side of equation (2), b indexes each nucleotide base (b = `A,T,C,G`) and f denotes the fluorescence score (see Processing sequencing reads) rounded to the nearest whole number ($f=1,2,3,4$). The expression $p_i(b)$ denotes the relative frequency of base b (`A`, `T`, `C`, or `G`) at position i . $p(f)$) is the relative frequency of a daughter sequence with a (rounded) fluorescence score of 1,2,3, or 4. $p_i(b,f)$ is the observed joint probability, i.e., the relative frequency of a daughter sequence having a score of f and base b at position i.

The right term on the right-hand side of equation (2) is a correction term for differences in degrees of freedom (9 degrees of freedom), where $n_b = 4$ is the number of possible bases $n_f = 4$ is the number of possible (rounded) fluorescence scores, and N is the size of the library. The fewer degrees of freedom there are and the larger the library is, the smaller the correction term.

For the mutual information plots shown in the text, we computed a Gaussian filter with the `ndimage` (alpha = 1) function in `scipy` (v1.8.1). In these plots, the solid line is always the average mutual information between r1, r2, and r3 at each position, and the lightly shaded region indicates ± 1 standard deviation between r1, r2, and r3 at each position.

Identifying mutual information hotspots

We calculated the mutual information for each parent and its daughters (see Mutual Information), and used the following procedure to automatically identify mutual information hotspots. First, we subtracted the standard deviation from the mean mutual information at each nucleotide position *i*, and truncated all values smaller than 0.0005 bits to 0 bits. We refer to the resulting quantity as *adjusted* mutual information. We then established the 90th percentile of this adjusted mutual information at each nucleotide position *i* as a threshold to identify mutual information hotspots. Specifically, we identified mutual information hotspots as nucleotide positions where the adjusted mutual information 1) lies above this threshold, and 2) is greater than the mutual information at the positions *i*-1 and *i*+1. See **Data S3** for hotspot coordinates.

Analysis of motif gain and loss

To identify hotspots in which gaining and losing a -10 or -35 box associates with a significant change in gene expression (fluorescence), we performed the following procedure. First, we drew a 6 bp sliding window starting at the beginning of each parent sequence. Within this window, we calculated the respective -10 and -35 PWM score for every daughter sequence (see **Fig S7A**). For each daughter sequence, if the binding score was greater than a designated threshold (-35 box = 3.39 bits, -10 box = 3.98 bits, see "Position Weight Matrices"), we added the fluorescence score to a "Motif (+)" list. If the PWM score was below this threshold, we added the score to a "Motif (-)" list (see **Fig S7B**).

If each list contained more than 10 values, we then tested the null hypothesis that the fluorescence scores have the same central tendency, using a two-sided Mann-Whitney U test (`mannwhitneyu` function from `scipy.stats`, v1.8.1). If the p-value was less than 0.05 and was located within ±3 bp from a hotspot, we recorded the value in **Data S4**. We then advanced the 6 bp window in steps of one nucleotide position until it had reached the final end of the

parent sequence, and repeated this calculation at each location of the sliding window. See **Fig S7**.

We performed this analysis for both GFP and RFP fluorescence scores on their respective DNA strands for both -10 and -35 boxes and for all 25 parent sequences (**Data S4)**. To account for multiple hypothesis testing, we calculated corrected q-values using a Benjamini-Hochberg correction (false-discovery rate 0.05).

For subsequent analyses, we only focused on significant associations found within ± 3 bp from the peak of each hotspot (see "Identifying promoter emergence hotspots" and "Mutual information"), and associations where the median fluorescence difference between the lists box present and box absent is larger than the absolute value of 0.5 arbitrary units (a.u.).

ACKNOWLEDGEMENTS AND CONTRIBUTIONS

The European Molecular Biology Organization (EMBO) supports TF with a postdoctoral fellowship (ALTF 963-2021). AW and his group is supported by the Swiss National Science Foundation (grants 310030_208174).

We would like to thank the Wagner lab for all discussions and conversations, even if they were not always pertinent to science. We additionally thank Baxter for inspiring Tim with the analysis pipeline during a painfully slow and cold morning walk.

REFERENCES

Afek A, Schipper JL, Horton J, Gordân R, Lukatsky DB. 2014. Protein−DNA binding in the absence of specific base-pair recognition. *Proceedings of the National Academy of Sciences* **111**:17140–17145. doi:10.1073/pnas.1410569111

Avsec Ž, Weilert M, Shrikumar A, Krueger S, Alexandari A, Dalal K, Fropf R, McAnany C, Gagneur J, Kundaje A, Zeitlinger J. 2021. Base-resolution models of transcription-factor binding reveal soft motif syntax. *Nat Genet* **53**:354–366. doi:10.1038/s41588-021-00782-6

Belliveau NM, Barnes SL, Ireland WT, Jones DL, Sweredoski MJ, Moradian A, Hess S, Kinney JB, Phillips R. 2018. Systematic approach for dissecting the molecular mechanisms of transcriptional regulation in bacteria. *Proceedings of the National Academy of Sciences* **115**:E4796–E4805. doi:10.1073/pnas.1722055115

Berman BP, Nibu Y, Pfeiffer BD, Tomancak P, Celniker SE, Levine M, Rubin GM, Eisen MB. 2002. Exploiting transcription factor binding site clustering to identify cis-regulatory modules involved in pattern formation in the Drosophila genome. *Proc Natl Acad Sci U S A* **99**:757–762. doi:10.1073/pnas.231608898

Burgess RR, Travers AA, Dunn JJ, Bautz EK. 1969. Factor stimulating transcription by RNA polymerase. *Nature* **221**:43–46. doi:10.1038/221043a0

Burr T, Mitchell J, Kolb A, Minchin S, Busby S. 2000. DNA sequence elements located immediately upstream of the –10 hexamer in Escherichia coli promoters: a systematic study. *Nucleic Acids Res* **28**:1864–1870.

Bykov A, Glazunova O, Alikina O, Sukharicheva N, Masulis I, Shavkunov K, Ozoline O. 2020. Excessive Promoters as Silencers of Genes Horizontally Acquired by Escherichia coli. *Front Mol Biosci* **7**:28. doi:10.3389/fmolb.2020.00028

Chauhan V, Bahrudeen MNM, Palma CSD, Baptista ISC, Almeida BLB, Dash S, Kandavalli V, Ribeiro AS. 2022. Analytical kinetic model of native tandem promoters in E. coli. *PLOS Computational Biology* **18**:e1009824. doi:10.1371/journal.pcbi.1009824

Chiu T-P, Li J, Jiang Y, Rohs R. 2022. It is in the flanks: Conformational flexibility of transcription factor binding sites. *Biophysical Journal* **121**:3765–3767. doi:10.1016/j.bpj.2022.09.020

Cock PJA, Antao T, Chang JT, Chapman BA, Cox CJ, Dalke A, Friedberg I, Hamelryck T, Kauff F, Wilczynski B, de Hoon MJL. 2009. Biopython: freely available Python tools for computational

molecular biology and bioinformatics. *Bioinformatics* **25**:1422–1423. doi:10.1093/bioinformatics/btp163

Crampton N, Bonass WA, Kirkham J, Rivetti C, Thomson NH. 2006. Collision events between RNA polymerases in convergent transcription studied by atomic force microscopy. *Nucleic Acids Research* **34**:5416–5425. doi:10.1093/nar/gkl668

Estrem ST, Gaal T, Ross W, Gourse RL. 1998. Identification of an UP element consensus sequence for bacterial promoters. *Proc Natl Acad Sci U S A* **95**:9761–9766.

Farley EK, Olson KM, Zhang W, Brandt AJ, Rokhsar DS, Levine MS. 2015. Suboptimization of developmental enhancers. *Science* **350**:325–328. doi:10.1126/science.aac6948

Fuqua T, Jordan J, van Breugel ME, Halavatyi A, Tischer C, Polidoro P, Abe N, Tsai A, Mann RS, Stern DL, Crocker J. 2020. Dense and pleiotropic regulatory information in a developmental enhancer. *Nature* **587**:235–239. doi:10.1038/s41586-020-2816-5

Galupa R, Alvarez-Canales G, Borst NO, Fuqua T, Gandara L, Misunou N, Richter K, Alves MRP, Karumbi E, Perkins ML, Kocijan T, Rushlow CA, Crocker J. 2023. Enhancer architecture and chromatin accessibility constrain phenotypic space during Drosophila development. *Developmental Cell* **58**:51-62.e4. doi:10.1016/j.devcel.2022.12.003

Gordân R, Shen N, Dror I, Zhou T, Horton J, Rohs R, Bulyk ML. 2013. Genomic regions flanking E-box binding sites influence DNA binding specificity of bHLH transcription factors through DNA shape. *Cell Rep* **3**:1093–1104. doi:10.1016/j.celrep.2013.03.014

Gotea V, Visel A, Westlund JM, Nobrega MA, Pennacchio LA, Ovcharenko I. 2010. Homotypic clusters of transcription factor binding sites are a key component of human promoters and enhancers. *Genome Res* **20**:565–577. doi:10.1101/gr.104471.109

Hertz GZ, Stormo GD. 1999. Identifying DNA and protein patterns with statistically significant alignments of multiple sequences. *Bioinformatics* **15**:563–577. doi:10.1093/bioinformatics/15.7.563

Hobson DJ, Wei W, Steinmetz LM, Svejstrup JQ. 2012. RNA polymerase II collision interrupts convergent transcription. *Mol Cell* **48**:365–374. doi:10.1016/j.molcel.2012.08.027

Huerta AM, Collado-Vides J. 2003. Sigma70 Promoters in Escherichia coli: Specific Transcription in Dense Regions of Overlapping Promoter-like Signals. *Journal of Molecular Biology* **333**:261–278. doi:10.1016/j.jmb.2003.07.017

Inukai S, Kock KH, Bulyk ML. 2017. Transcription factor–DNA binding: beyond binding site motifs. *Curr Opin Genet Dev* **43**:110–119. doi:10.1016/j.gde.2017.02.007

Ireland WT, Beeler SM, Flores-Bautista E, McCarty NS, Röschinger T, Belliveau NM, Sweredoski MJ, Moradian A, Kinney JB, Phillips R. 2020. Deciphering the regulatory genome of Escherichia coli, one hundred promoters at a time. *eLife* **9**:e55308. doi:10.7554/eLife.55308

Jacob F, Monod J. 1961. Genetic regulatory mechanisms in the synthesis of proteins. *Journal of Molecular Biology* **3**:318–356. doi:10.1016/S0022-2836(61)80072-7

Kinney JB, Murugan A, Callan CG, Cox EC. 2010. Using deep sequencing to characterize the biophysical mechanism of a transcriptional regulatory sequence. *Proceedings of the National Academy of Sciences* **107**:9158–9163. doi:10.1073/pnas.1004290107

Klein CA, Teufel M, Weile CJ, Sobetzko P. 2021. The bacterial promoter spacer modulates promoter strength and timing by length, TG-motifs and DNA supercoiling sensitivity. *Sci Rep* **11**:24399. doi:10.1038/s41598-021-03817-4

Krieger G, Lupo O, Wittkopp P, Barkai N. 2022. Evolution of transcription factor binding through sequence variations and turnover of binding sites. *Genome Res* **32**:1099–1111. doi:10.1101/gr.276715.122

Lagator M, Sarikas S, Steinrueck M, Toledo-Aparicio D, Bollback JP, Guet CC, Tkačik G. 2022. Predicting bacterial promoter function and evolution from random sequences. *eLife* **11**:e64543. doi:10.7554/eLife.64543

Lässig M, Mustonen V, Walczak AM. 2017. Predicting evolution. *Nat Ecol Evol* **1**:1–9. doi:10.1038/s41559-017-0077

Lifanov AP, Makeev VJ, Nazina AG, Papatsenko DA. 2003. Homotypic Regulatory Clusters in Drosophila. *Genome Res* **13**:579–588. doi:10.1101/gr.668403

Loell KJ, Friedman RZ, Myers CA, Corbo JC, Cohen BA, White MA. 2024. Transcription factor interactions explain the context-dependent activity of CRX binding sites. *PLoS Comput Biol* **20**:e1011802. doi:10.1371/journal.pcbi.1011802

Lynch VJ, Nnamani MC, Kapusta A, Brayer K, Plaza SL, Mazur EC, Emera D, Sheikh SZ, Grützner F, Bauersachs S, Graf A, Young SL, Lieb JD, DeMayo FJ, Feschotte C, Wagner GP. 2015. Ancient Transposable Elements Transformed the Uterine Regulatory Landscape and Transcriptome during the Evolution of Mammalian Pregnancy. *Cell Reports* **10**:551–561. doi:10.1016/j.celrep.2014.12.052

Magoč T, Salzberg SL. 2011. FLASH: fast length adjustment of short reads to improve genome assemblies. *Bioinformatics* **27**:2957–2963. doi:10.1093/bioinformatics/btr507

Mendoza-Vargas A, Olvera L, Olvera M, Grande R, Vega-Alvarado L, Taboada B, Jimenez-Jacinto V, Salgado H, Juárez K, Contreras-Moreira B, Huerta AM, Collado-Vides J, Morett E. 2009. Genome-Wide Identification of Transcription Start Sites, Promoters and Transcription Factor Binding Sites in E. coli. *PLoS One* **4**:e7526. doi:10.1371/journal.pone.0007526

Mitchell JE, Zheng D, Busby SJW, Minchin SD. 2003. Identification and analysis of 'extended –10' promoters in Escherichia coli. *Nucleic Acids Res* **31**:4689–4695.

Paget MS, Helmann JD. 2003. The σ70family of sigma factors. *Genome Biology* **4**:203. doi:10.1186/gb-2003-4-1-203

Panyukov VV, Ozoline ON. 2013. Promoters of Escherichia coli versus Promoter Islands: Function and Structure Comparison. *PLOS ONE* **8**:e62601. doi:10.1371/journal.pone.0062601

Perales M, Rodriguez K, Snipes S, Yadav RK, Diaz-Mendoza M, Reddy GV. 2016. Threshold-dependent transcriptional discrimination underlies stem cell homeostasis. *Proc Natl Acad Sci U S A* **113**:E6298–E6306. doi:10.1073/pnas.1607669113

Peterman N, Levine E. 2016. Sort-seq under the hood: implications of design choices on large-scale characterization of sequence-function relations. *BMC Genomics* **17**:206. doi:10.1186/s12864-016-2533-5

Pribnow D. 1975. Nucleotide sequence of an RNA polymerase binding site at an early T7 promoter. *Proc Natl Acad Sci U S A* **72**:784–788.

Prud'homme B, Gompel N, Carroll SB. 2007. Emerging principles of regulatory evolution. *Proceedings of the National Academy of Sciences* **104**:8605–8612. doi:10.1073/pnas.0700488104

Purtov YA, Glazunova OA, Antipov SS, Pokusaeva VO, Fesenko EE, Preobrazhenskaya EV, Shavkunov KS, Tutukina MN, Lukyanov VI, Ozoline ON. 2014. Promoter islands as a platform for interaction with nucleoid proteins and transcription factors. *J Bioinform Comput Biol* **12**:1441006. doi:10.1142/S0219720014410066

Rebeiz M, Jikomes N, Kassner VA, Carroll SB. 2011. Evolutionary origin of a novel gene expression pattern through co-option of the latent activities of existing regulatory sequences. *Proceedings of the National Academy of Sciences* **108**:10036–10043. doi:10.1073/pnas.1105937108

Seshasayee ASN, Sivaraman K, Luscombe NM. 2011. An overview of prokaryotic transcription factors : a summary of function and occurrence in bacterial genomes. *Subcell Biochem* **52**:7–23. doi:10.1007/978-90-481-9069-0_2

Shavkunov KS, Masulis IS, Tutukina MN, Deev AA, Ozoline ON. 2009. Gains and unexpected lessons from genome-scale promoter mapping. *Nucleic Acids Res* **37**:4919–4931. doi:10.1093/nar/gkp490

Stern DL, Orgogozo V. 2008. The loci of evolution: how predictable is genetic evolution? *Evolution* **62**:2155–2177. doi:10.1111/j.1558-5646.2008.00450.x

Tierrafría VH, Rioualen C, Salgado H, Lara P, Gama-Castro S, Lally P, Gómez-Romero L, Peña-Loredo P, López-Almazo AG, Alarcón-Carranza G, Betancourt-Figueroa F, Alquicira-Hernández S, Polanco-Morelos JE, García-Sotelo J, Gaytan-Nuñez E, Méndez-Cruz C-F, Muñiz LJ, Bonavides-

Martínez C, Moreno-Hagelsieb G, Galagan JE, Wade JT, Collado-Vides J 2022. 2022. RegulonDB 11.0: Comprehensive high-throughput datasets on transcriptional regulation in Escherichia coli K-12. *Microbial Genomics* **8**:000833. doi:10.1099/mgen.0.000833

Timothy Fuqua, Andreas Wagner. 2023. Mobile DNA is replete with hotspots for the de novo emergence of gene regulation. *bioRxiv* 2023.10.22.563463. doi:10.1101/2023.10.22.563463

Urtecho G, Insigne KD, Tripp AD, Brinck MS, Lubock NB, Acree C, Kim H, Chan T, Kosuri S. 2023. Genome-wide Functional Characterization of Escherichia coli Promoters and Sequence Elements Encoding Their Regulation. *eLife* **12**. doi:10.7554/eLife.92558

Urtecho G, Tripp AD, Insigne KD, Kim H, Kosuri S. 2019. Systematic Dissection of Sequence Elements Controlling σ70 Promoters Using a Genomically Encoded Multiplexed Reporter Assay in Escherichia coli. *Biochemistry* **58**:1539–1551. doi:10.1021/acs.biochem.7b01069

van Hijum SAFT, Medema MH, Kuipers OP. 2009. Mechanisms and Evolution of Control Logic in Prokaryotic Transcriptional Regulation. *Microbiology and Molecular Biology Reviews* **73**:481–509. doi:10.1128/MMBR.00037-08

Villanueva-Cañas JL, Horvath V, Aguilera L, González J. 2019. Diverse families of transposable elements affect the transcriptional regulation of stress-response genes in Drosophila melanogaster. *Nucleic Acids Res* **47**:6842–6857. doi:10.1093/nar/gkz490

Villar D, Berthelot C, Aldridge S, Rayner TF, Lukk M, Pignatelli M, Park TJ, Deaville R, Erichsen JT, Jasinska AJ, Turner JMA, Bertelsen MF, Murchison EP, Flicek P, Odom DT. 2015. Enhancer evolution across 20 mammalian species. *Cell* **160**:554–566. doi:10.1016/j.cell.2015.01.006

Wang L, Watters JW, Ju X, Lu G, Liu S. 2023. Head-on and co-directional RNA polymerase collisions orchestrate bidirectional transcription termination. *Molecular Cell* **83**:1153-1164.e4. doi:10.1016/j.molcel.2023.02.017

Warman EA, Forrest D, Guest T, Haycocks JJRJ, Wade JT, Grainger DC. 2021. Widespread divergent transcription from bacterial and archaeal promoters is a consequence of DNA-sequence symmetry. *Nat Microbiol* **6**:746–756. doi:10.1038/s41564-021-00898-9

Westmann CA, Alves L de F, Silva-Rocha R, Guazzaroni M-E. 2018. Mining Novel Constitutive Promoter Elements in Soil Metagenomic Libraries in Escherichia coli. *Frontiers in Microbiology* **9**.

Yue F, Cheng Y, Breschi A, Vierstra J, Wu W, Ryba T, Sandstrom R, Ma Z, Davis C, Pope BD, Shen Y, Pervouchine DD, Djebali S, Thurman RE, Kaul R, Rynes E, Kirilusha A, Marinov GK, Williams BA, Trout D, Amrhein H, Fisher-Aylor K, Antoshechkin I, DeSalvo G, See L-H, Fastuca M, Drenkow J, Zaleski C, Dobin A, Prieto P, Lagarde J, Bussotti G, Tanzer A, Denas O, Li K, Bender MA, Zhang M, Byron R, Groudine MT, McCleary D, Pham L, Ye Z, Kuan S, Edsall L, Wu Y-C, Rasmussen MD, Bansal MS, Kellis M, Keller CA, Morrissey CS, Mishra T, Jain D, Dogan N, Harris RS, Cayting P, Kawli T, Boyle AP, Euskirchen G, Kundaje A, Lin S, Lin Y, Jansen C, Malladi VS, Cline MS, Erickson DT, Kirkup VM, Learned K, Sloan CA, Rosenbloom KR, Lacerda de Sousa B, Beal K, Pignatelli M, Flicek P, Lian J, Kahveci T, Lee D, Kent WJ, Ramalho Santos M, Herrero J, Notredame C, Johnson A, Vong S, Lee K, Bates D, Neri F, Diegel M, Canfield T, Sabo PJ, Wilken MS, Reh TA, Giste E, Shafer A, Kutyavin T, Haugen E, Dunn D, Reynolds AP, Neph S, Humbert R, Hansen RS, De Bruijn M, Selleri L, Rudensky A, Josefowicz S, Samstein R, Eichler EE, Orkin SH, Levasseur D, Papayannopoulou T, Chang K-H, Skoultchi A, Gosh S, Disteche C, Treuting P, Wang Y, Weiss MJ, Blobel GA, Cao X, Zhong S, Wang T, Good PJ, Lowdon RF, Adams LB, Zhou X-Q, Pazin MJ, Feingold EA, Wold B, Taylor J, Mortazavi A, Weissman SM, Stamatoyannopoulos JA, Snyder MP, Guigo R, Gingeras TR, Gilbert DM, Hardison RC, Beer MA, Ren B, Mouse ENCODE Consortium. 2014. A comparative encyclopedia of DNA elements in the mouse genome. *Nature* **515**:355–364. doi:10.1038/nature13992

871 **SUPPLEMENTARY FIGURES**

872

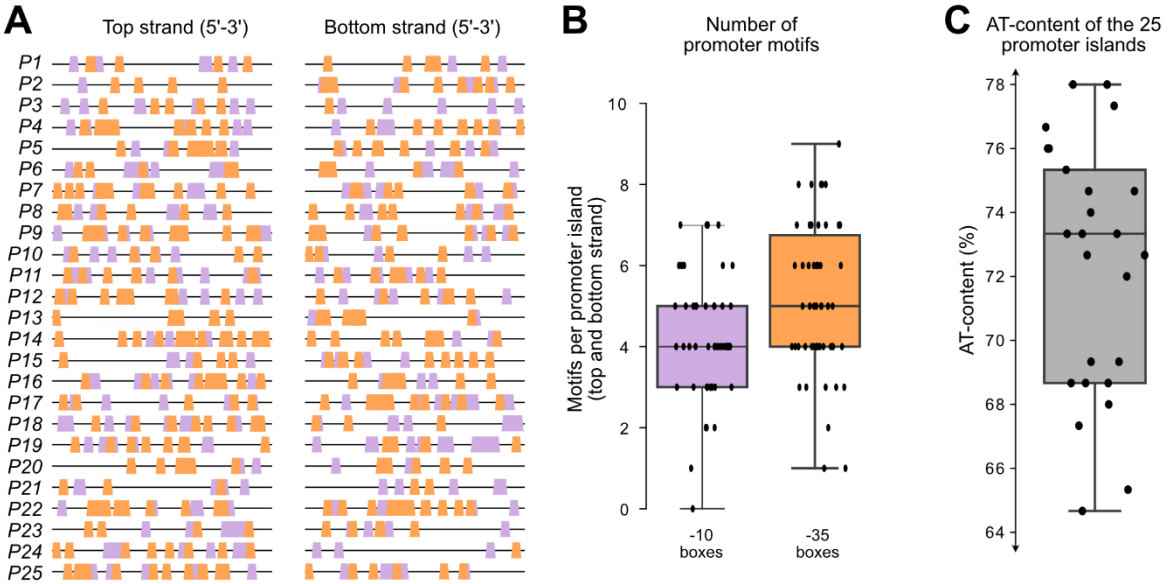

873

874 **Figure S1. Promoter island sequences. (A)** The locations and arrangements of -10 and -35 box motifs located
875 across both the top and bottom strands of the 150 base pair DNA sequences called parent sequences (P1-P25).
876 Orange trapezoids: -35 box motifs. Magenta trapezoids: 10 box motifs. Left: top strand. Right: bottom strand. Note:
877 the plot is shown from 5'-3' for both strands. **(B)** Distributions for the number of motifs found in the 25 promoter
878 island sequences. We identified motifs with position-weight matrices (PWMs, methods). Magenta: the number of -
879 10 box motifs in each promoter island regardless of orientation (n=50). Orange: the number of -35 box motifs in
880 each promoter island, in both orientations (n=50). **(C)** Distribution of AT-content for the 25 parent sequences. Boxes
881 in B) and C) represent the interquartile range (IQR) and the center line the median. Whiskers correspond to 1.5×IQR

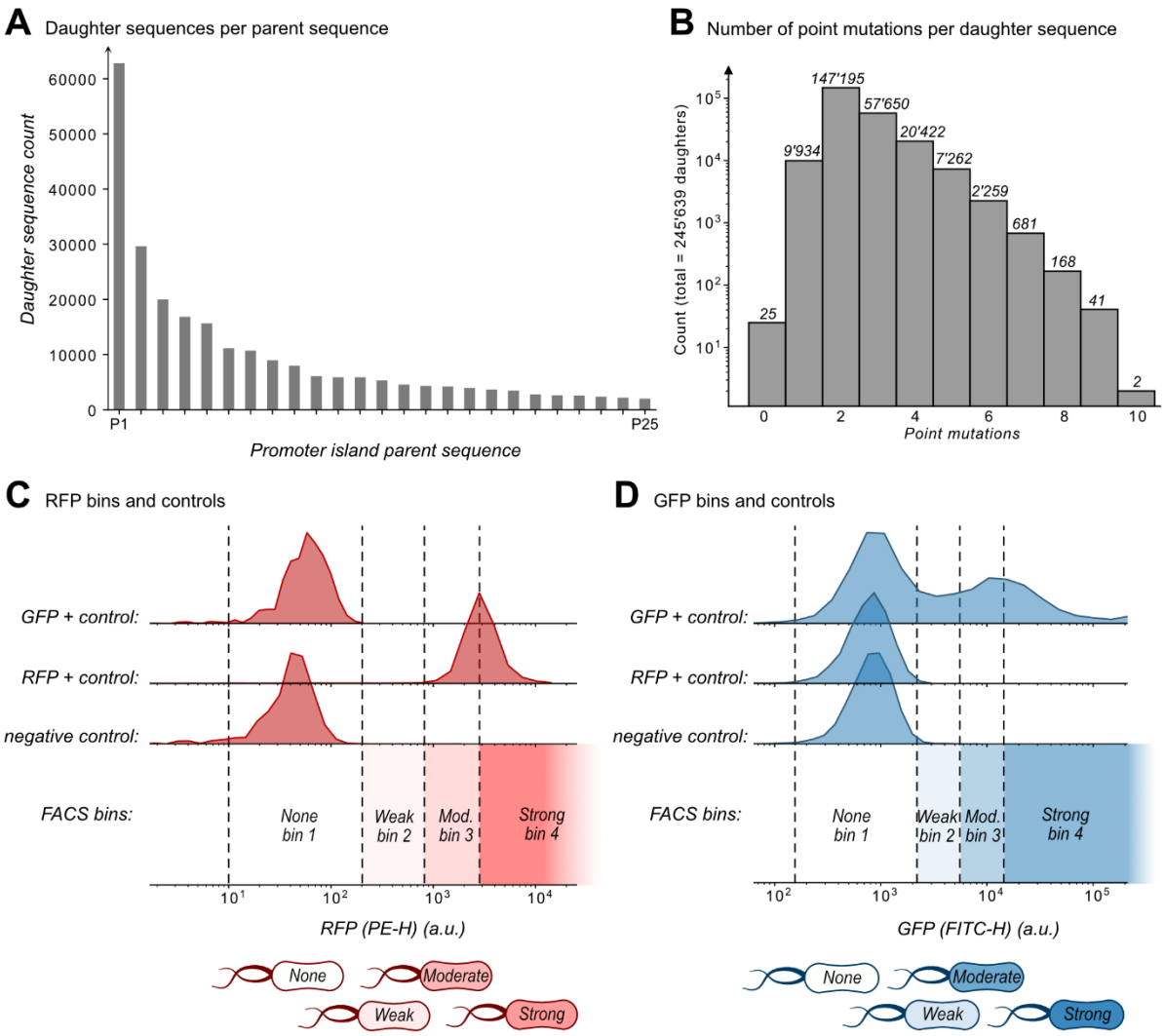

Figure S2. Mutagenesis library and sort-seq bins. (A) A histogram with the number of unique daughter sequences per parent sequence (N=245'639). **(B)** The number of point mutations per daughter sequence (N=245'639). The number above each bin is the number of daughters in each bin. **(C)** We defined four red fluorescence bins (1, 2, 3, 4, corresponding to none, weak, moderate, and strong fluorescence, respectively) using three controls: GFP+, RFP+, and a negative control (see Methods). Plots show histograms of the fluorescent readouts from 10'000 cells for each control. For bin 1 (none), we defined a minimum boundary as the larger of two PE-H values. These values are the minimum PE-H of the negative control (empty pMR1 plasmid) and the minimum PE-H of the opposite fluorophore positive control (GFP in this case). The upper boundary of bin 1 is the highest PE-H value detected for these same controls. For bin 4 (strong), we defined the lower boundary as the mean fluorescence level of the positive RFP control. This bin does not have an upper bound, because it encompasses the highest levels of fluorescence. For RFP bins 2 (weak) and 3 (moderate), the lower bound of bin 2 is identical to the upper bound of bin 1. The upper bound of bin 3 is identical to the lower bound of bin 4. The upper bound of bin 2, which is identical to the lower bound of bin 3, equals the average of the lower boundary of bin 4 and the upper bound of bin 1. **(D)** Analogous to (C) except with GFP and RFP controls swapped, with the following exception: Because the GFP positive control produces a bimodal FITC-H distribution, we defined the lower bound of bin 4 for green fluorescence as the peak of the higher mode of this distribution.

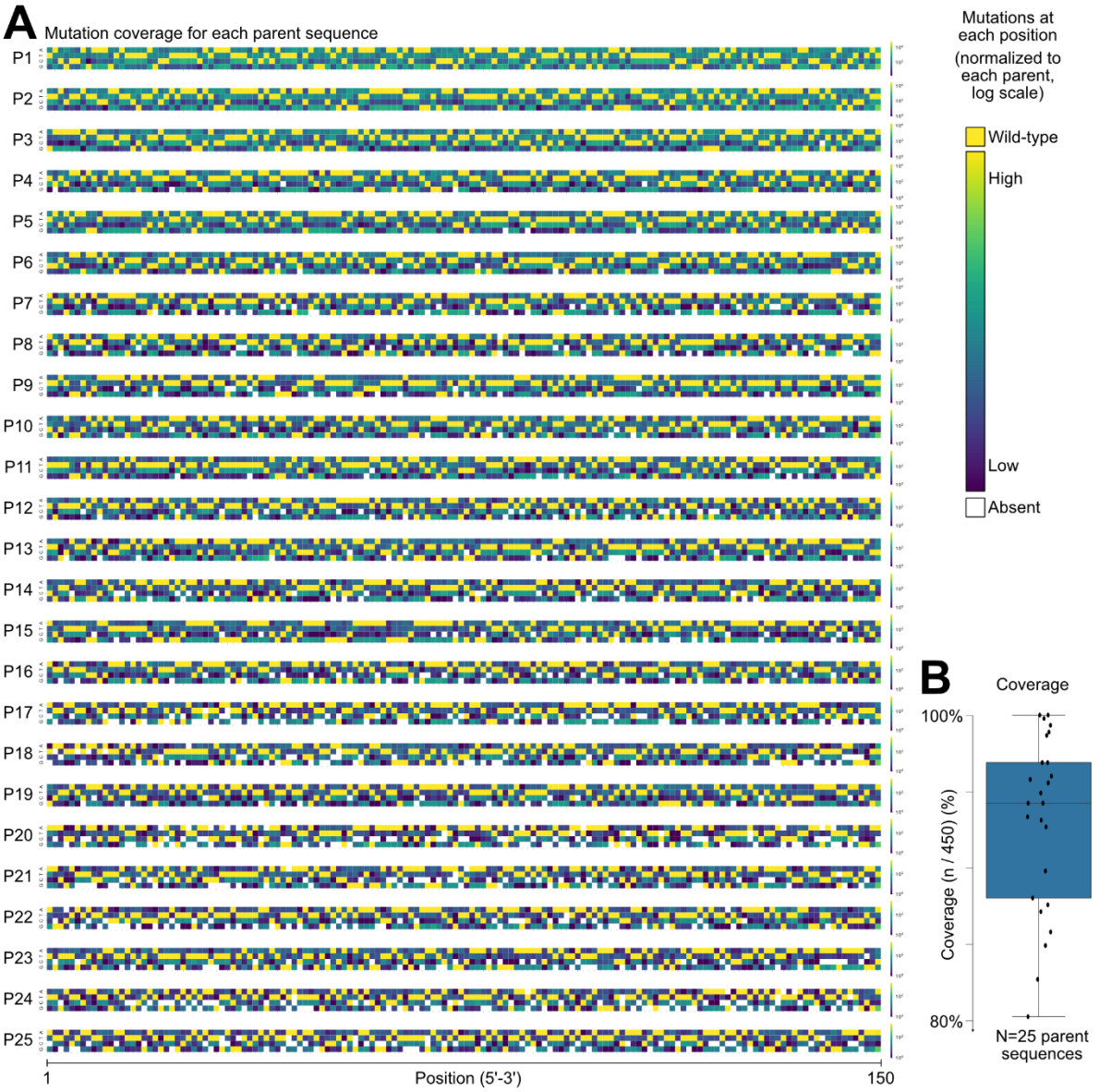

Figure S3. Mutational coverage for the parent sequences. (A) Heatmaps depicting the frequency of each nucleotide (A,T,C,G, y-axis) at each position (5'-3', x-axis) for all of the daughter sequences of each parent sequence (P1-P25). Daughter sequences contain 1-10 point mutations (see **Fig S2B**). The color of each square in the heatmap corresponds to the frequency of each nucleotide occurring in the library at its respective position, where less frequent nucleotides are shown in dark magenta. Highly frequent nucleotides are in yellow (log-scale). These include the nucleotides of the parent sequence, due to our modest mutation rate (~2.0 point mutations per daughter sequence). Light gray squares indicate mutations absent from the library. **(B)** We calculate coverage as the percentage of all possible mutations of the parent sequences (A,T,C,G and positions 1 through 150, 3×150 = 450 total neighboring mutations). In the boxplot, the box represents the interquartile range (IQR) and the center line the median. Whiskers correspond to 1.5×IQR.

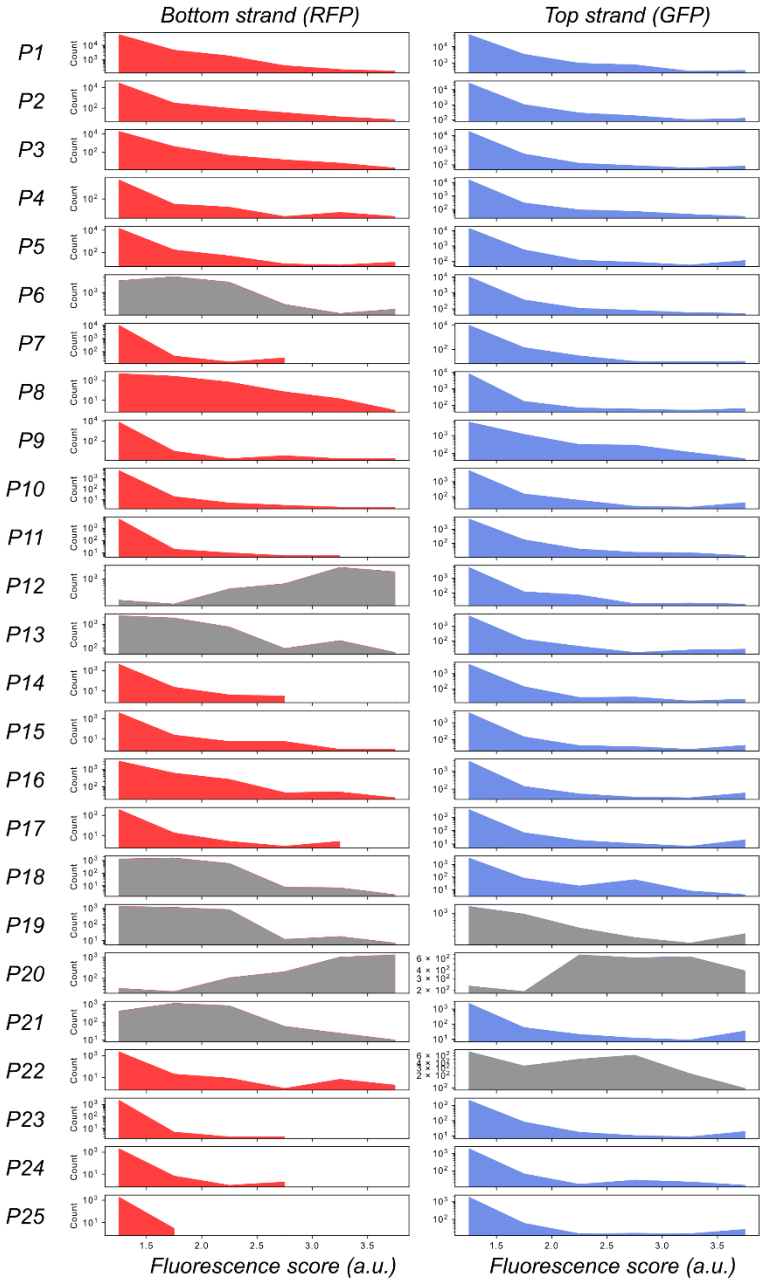

Figure S4. Histogram of the fluorescence score distributions for each promoter island and genetic orientation. Rows: parent sequences (P1-P25). Left column: bottom strand (RFP fluorescence scores); Right column: top strand (GFP fluorescence scores.) Each panel is a histogram of the frequency of fluorescence scores (arbitrary units, a.u.) from the sort-seq experiment. Gray histograms indicate those parent sequences / orientations that already encode promoter activity. Note: daughter sequence counts vary among parents, and y-axis is unique to each panel.

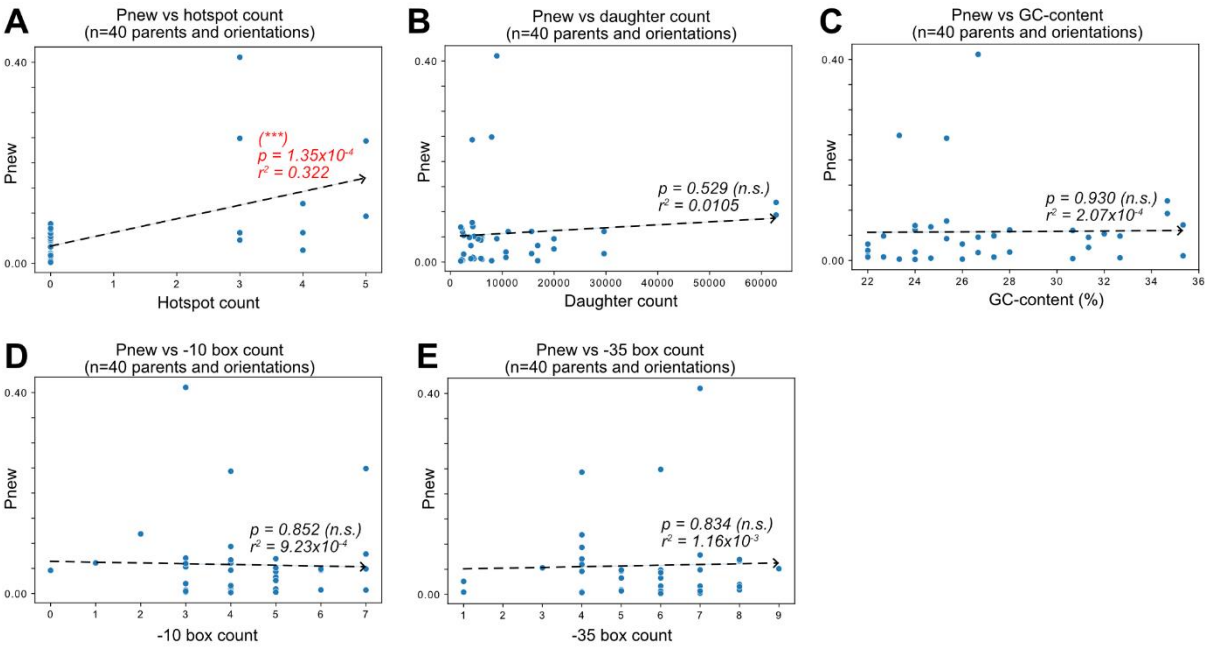

Figure S5. Number of hotspots correlates with P_{new}, but numbers of -10 and -35 box motifs do not. (A) Scatterplots comparing the number of mutual information hotspots (see **Fig 2**) and P_{new} (see **Fig 1**). P_{new} is the ratio of daughter sequences with a fluorescence score greater than 1.5 a.u. to the total number of daughter sequences for each parent. Each point represents a parent / orientation without regulatory activity (n=40). The dotted line is the line of best fit calculated using the method of least squares. We test the null hypothesis that the slope of the correlation equals zero with the Wald Test. The r^2 value is the Pearson correlation coefficient. Calculation carried out using `scipy.stats.linregress` (version 1.8.1) ($p=1.35\times10^{-4}$, $r^2=0.322$). **(B)** Analogous to (A) but comparing the number of daughter sequences for each parent with P_{new} ($p=0.529$, $r^2=0.0105$, n.s.). **(C)** Analogous to (A) but comparing the GC-content of each parent sequence with P_{new} ($p=0.930$, $r^2=2.07\times10^{-4}$, not significant (n.s.)). **(D)** Analogous to (A) but comparing the number of -10 box motifs in each parent sequence and orientation with P_{new} ($p=0.852$, $r^2=9.23\times10^{-4}$, n.s.). **(E)** Analogous to (A) but comparing the number of -35 box motifs in each parent sequence and orientation with P_{new} ($p=0.834$, $r^2=1.16\times10^{-3}$, n.s.).

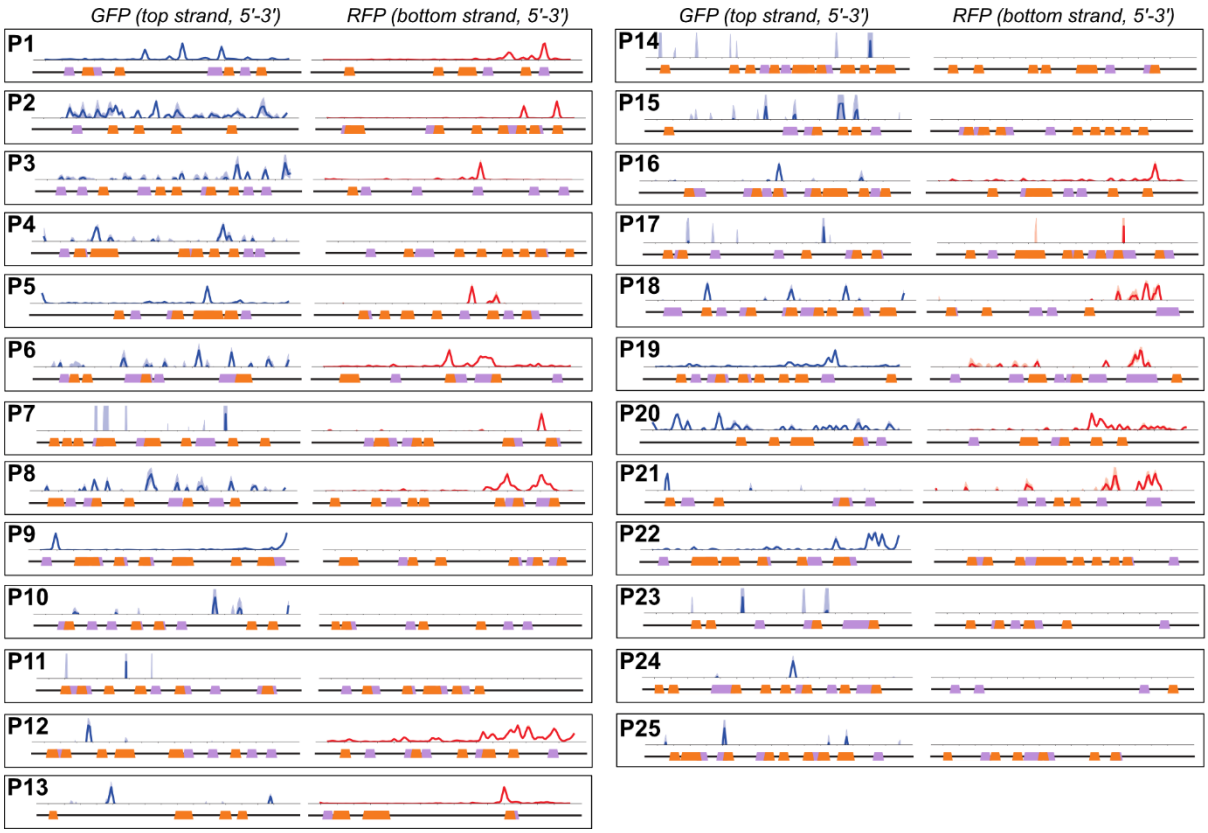

Figure S6. Mutual information and promoter motifs in the promoter islands. Each panel corresponds to a unique promoter island sequence, with its numerical identifier in bold. Within each panel there are two plots, corresponding to the top strand (left), and the bottom strand (right), both shown from 5' (left) to 3' (right). Within each panel, we show on top the mutual information $I_i(b, f)$ between nucleotide identity and fluorescence levels at every position (Solid line: mean mutual information, shaded region: ± 1 standard deviation when the dataset is randomly split into three equally sized subsets (methods)). The bottom of each panel shows position-weight matrix (PWM) predictions for the occurrence of -10 box motifs (magenta trapezoids) and -35 box motifs (orange trapezoids) along the wild-type parent sequence. See methods.

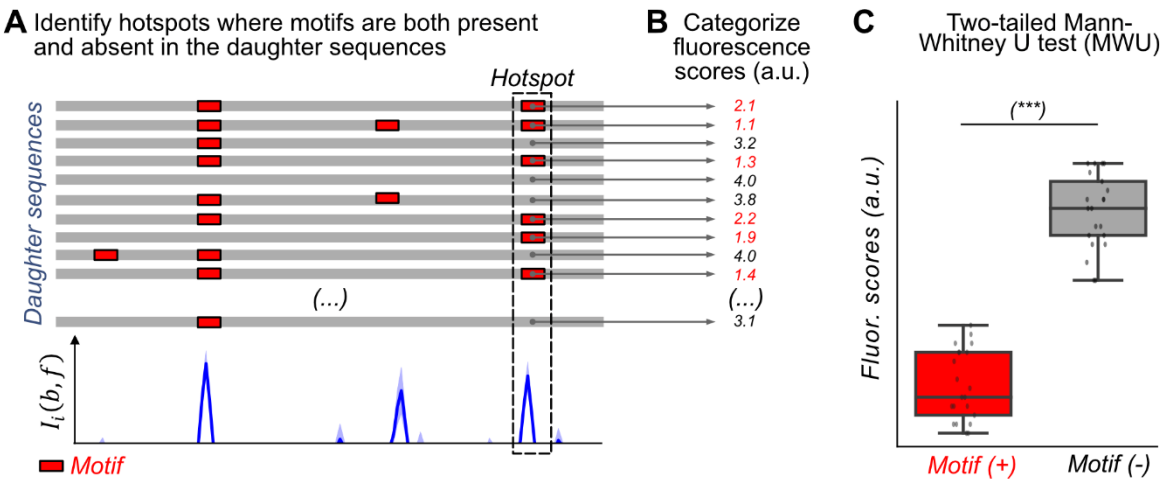

Figure S7. Identifying where motifs are gained and lost in hotspots that are associated with changes in fluorescence. These panels do not show data from any parent sequence or hotspot, but show hypothetical data to illustrate how we identified the associations of base identity and fluorescence in our analysis. **(A)** Top: a cartoon illustration of all daughter sequences from a single parent. Red boxes correspond to position-weight matrix (PWM) predicted motifs. Bottom: Mutual information between fluorescence levels and nucleotide identity at each position calculated from the respective daughter sequences of a given parent sequence. We examine for each mutual information hotspot if -35 or -10 box motifs are present or absent in each daughter sequence. The dashed rectangle highlights a hotspot at the 3'-end of the daughter sequences discussed in B) and C). **(B)** We categorize the fluorescence scores for the daughter sequences based on whether they have a motif (red) or not (black) in the hotspot. **(C)** We test the null hypothesis that the fluorescence scores in each group have the same central tendency using a two-sided Mann-Whitney U (MWU) test. See methods.

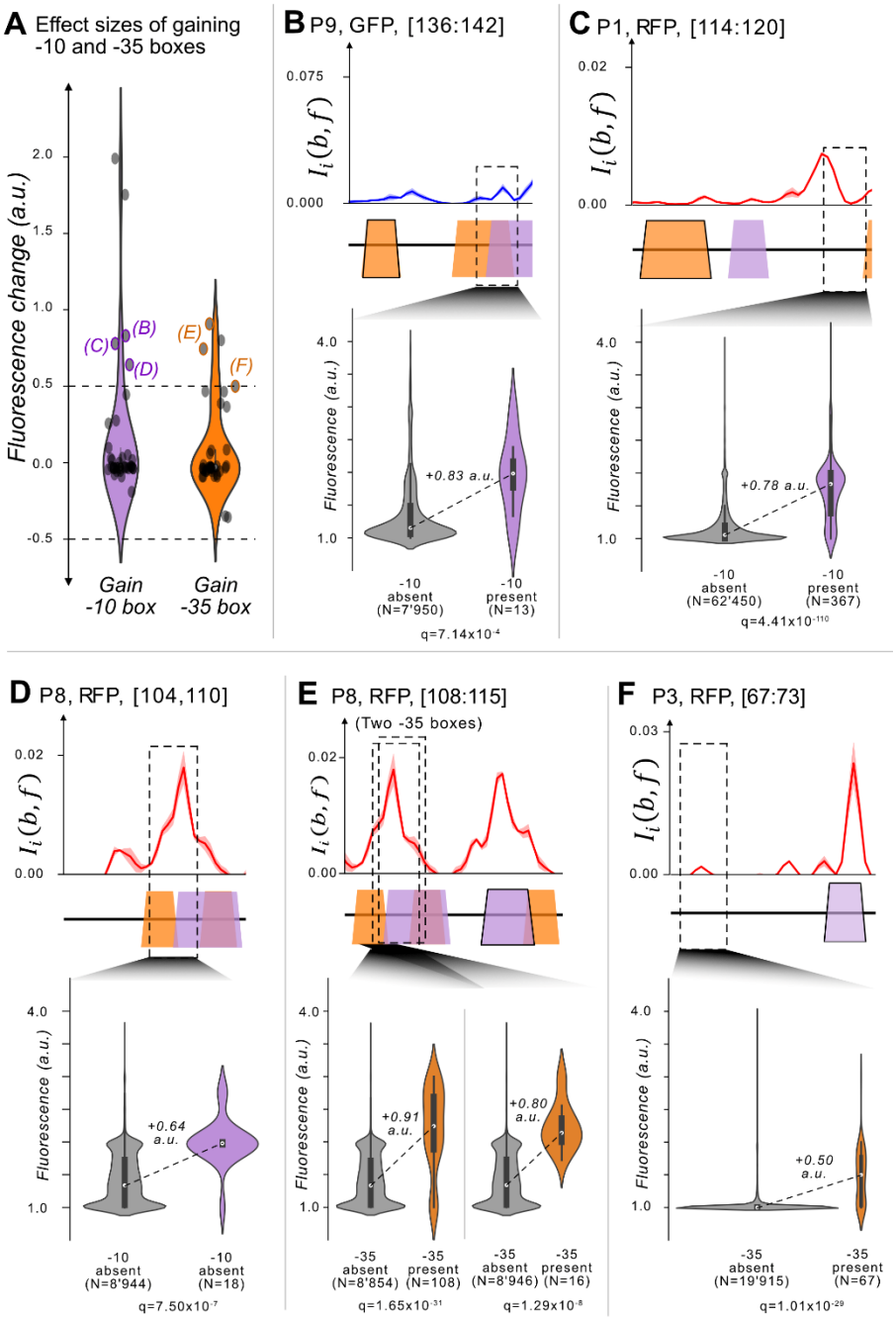

952

953 **Figure S8. Additional examples of which gaining -10 and -35 boxes creates de-novo promoters.** (**A**) The
954 change in fluorescence (arbitrary units, a.u.) when gaining or losing -10 and -35 boxes in hotspots in the non-
955 regulatory parent sequences. Dotted lines indicate an effect size threshold of ± 0.5 a.u. Each point corresponds to
956 a gain or loss of a motif in a mutual information hotspot. Outlined points with letters in parenthesis highlight the
957 corresponding figure panels. See **Fig 3A** for the same plot. The areas of the violin plots are the kernel density
958 estimates (KDE) of each distribution. **(B)** Top: the top strand of parent P9. Dashed rectangle indicates the region
959 of interest analyzed in the subsequent figure panel. We plot the mutual information $I_i(b,f)$ between nucleotide
960 identity and fluorescence at each position. Solid line: mean mutual information, shaded region: ± 1 standard
961 deviation when the dataset is randomly split into three equally sized subsets (methods). Middle: position-weight
962 matrix (PWM) predictions for the -10 box motifs (magenta trapezoids) and -35 box motifs (orange trapezoids) along
963 the wild-type parent sequence. Bottom: fluorescence scores (a.u.) for daughter sequences with vs without a -10
964 box in the region of interest at position 136:142. We tested the null hypothesis that the fluorescence scores have
965 the same central tendency using a two-sided Mann-Whitney U (MWU) test ($q=7.14\times10^{-4}$). The areas of the violin
966 plots are the kernel density estimates (KDE) of each distribution. Within each violin plot is a box plot. The box
967 represent the interquartile range (IQR) and the center line the median. Whiskers correspond to 1.5×IQR. **(C)**

Analogous to (B) except for gaining a -10 box on the bottom strand of parent P1 at position 114:120 (two-tailed MWU test, $q=4.41\times10^{-110}$). **(D)** Analogous to (B) except for gaining a -10 box on the bottom strand of parent P8 at position 104:110 (two-tailed MWU test, $q=7.50\times10^{-7}$). **(E)** Analogous to (B) except for gaining two -35 boxes on the bottom strand of parent P8 at position 108:115 (two-tailed MWU tests, $q=1.65\times10^{-31}$ and $q=1.29\times10^{-8}$, left and right -35 box, respectively). **(F)** Analogous to (B) except for gaining a -35 box on the top strand of parent P3 at position 16:22 (two-tailed MWU test, $q=9.62\times10^{-15}$).

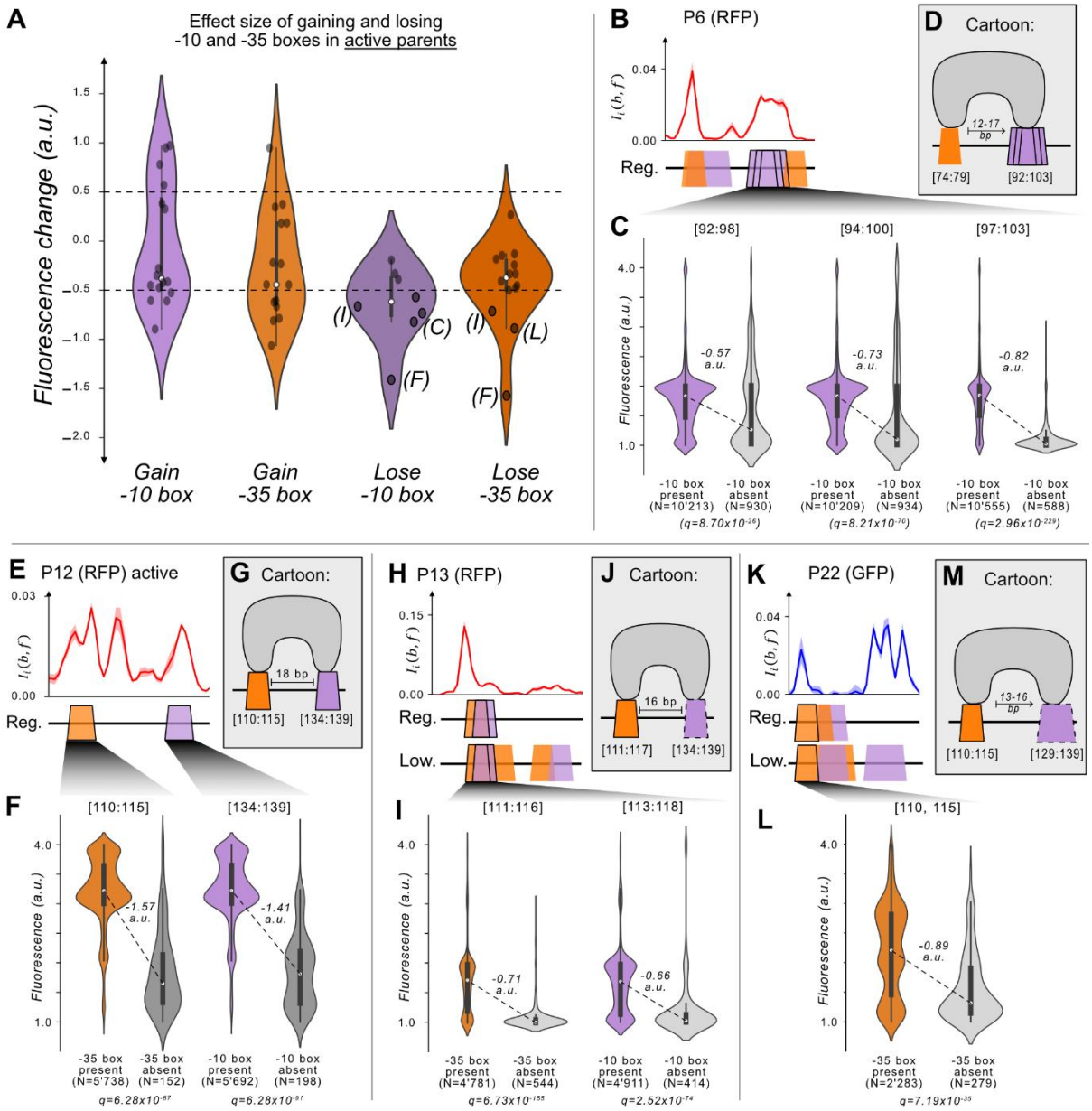

Figure S9. Mapping promoters in active parents. (**A**) The change in fluorescence (arbitrary units, a.u.) when gaining or losing -10 and -35 boxes in hotspots in the active parent sequences. Dotted lines indicate an effect size threshold of ± 0.5 a.u. Each point corresponds to a gain or loss of a -10 or -35 box in a mutual information hotspot. Outlined points with letters in parenthesis highlight the corresponding figure panels. The areas of the violin plots are the kernel density estimates (KDE) of each distribution. Within each violin plot is a box plot, where the box represents the interquartile range (IQR) and the white circle the median. Whiskers correspond to 1.5×IQR. **(B)** Top: the bottom strand of parent P6. We plot the mutual information $I_i(b,f)$ between nucleotide identity and fluorescence at each position. Solid line: mean mutual information, shaded region: ± 1 standard deviation when the dataset is randomly split into three equally sized subsets (methods). Middle: position-weight matrix (PWM) predictions for the -10 box motifs (magenta trapezoids) and -35 box motifs (orange trapezoids) along the wild-type parent sequence. Outlined trapezoids with shadows indicate regions of interest for the subsequent figure panel. **(C)** We test the null hypothesis that the fluorescence scores have the same central tendency for daughter sequences with vs without -10 boxes using a two-sided Mann-Whitney U (MWU) test. We tested the gain of -10 boxes in three locations. Left: position 92:98 ($q=8.70\times10^{-25}$), middle: position 94:100 ($q=8.21\times10^{-70}$), right: position 97:103 ($q=2.96\times10^{-229}$). **(D)** We combine the information from the previous panels (B-C) to generate a cartoon model for P6. Solid trapezoids correspond to validated binding sites in the previous panel. Trapezoids without borders correspond to PWM predicted motifs. Dashed trapezoids refer to inferred low-affinity motifs (see methods). Orange trapezoids: -35 boxes, magenta trapezoids = -10 boxes. **(E)** Analogous to (B) but for the bottom strand of P12. **(F)** Analogous to (C) but for losing a -35 box and a -10 box (two-tailed MWU test, $q=6.29\times10^{-67}$ and $q=5.28\times10^{-91}$, respectively). **(G)**

Analogous to (D) but a cartoon model for P12 based on panels (E-F). **(H)** Analogous to (B) but for the bottom strand of P13. **(I)** Analogous to (C) but for losing a -35 box and a -10 box (two-tailed MWU test, $q=6.73\times10^{-155}$ and $q=2.52\times10^{-74}$, respectively). **(J)** Analogous to (D) but a cartoon model for P13 based on panels (H-I). **(K)** Analogous to (B) but for the top strand of P22. **(L)** Analogous to (C) but for losing a -35 box (two-tailed MWU test, $q=7.19\times10^{-35}$). **(M)** Analogous to (D) but a cartoon model for P22 based on panels (K-L).

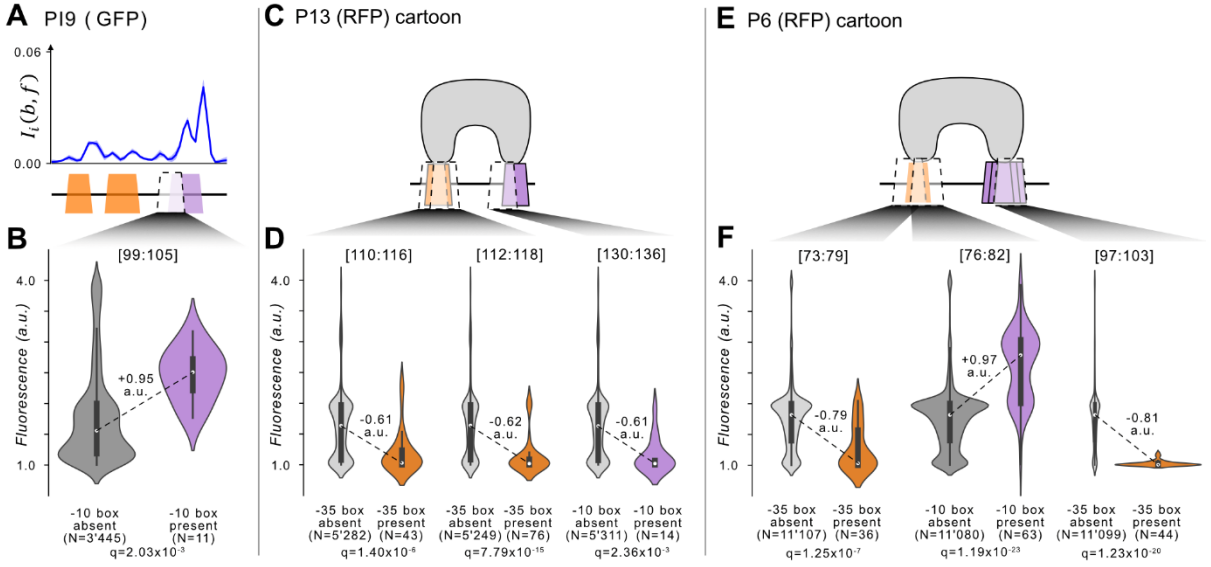

Figure S10. Additional examples of mutations modulating promoter activity. (**A**) Top: the top strand of parent P19. We plot the mutual information $I_i(b,f)$ between nucleotide identity and fluorescence at each position. Solid line: mean mutual information, shaded region: ± 1 standard deviation when the dataset is randomly split into three equally sized subsets (methods). Middle: position-weight matrix (PWM) predictions for the -10 box motifs (magenta trapezoids) and -35 box motifs (orange trapezoids) along the wild-type parent sequence. Dashed trapezoids with shadows indicate regions of interest for the subsequent figure panel. **(B)** We test the null hypothesis that the fluorescence scores have the same central tendency for daughter sequences with vs without -10 boxes using a two-sided Mann-Whitney U (MWU) test ($q=2.03\times10^{-3}$). The areas of the violin plots are the kernel density estimates (KDE) of each distribution. Within each violin plot is a box plot, where the box represents the interquartile range (IQR) and the white circle the median. Whiskers correspond to 1.5×IQR. **(C)** A cartoon for the promoter mapped on the bottom strand of P13 based on data from **Fig S9**. Orange trapezoids = -35 boxes, magenta trapezoids = -10 boxes, dashed trapezoids = regions of interest in subsequent figure panels. **(D)** Analogous to (B) but for gaining (left) a -35 box, (middle) a -35 box, (right) a -10 box (two-sided MWU test, $q=1.40\times10^{-6}$, $q=7.79\times10^{-15}$, $q=2.36\times10^{-3}$, respectively). **(E)** Analogous to (C) but for the bottom strand of P6. **(F)** Analogous to (B) but for gaining (left) a -35 box, (middle) a -10 box, (right) a -35 box (two-sided MWU test, $q=1.25\times10^{-7}$, $q=1.19\times10^{-23}$, $q=1.23\times10^{-20}$, respectively).

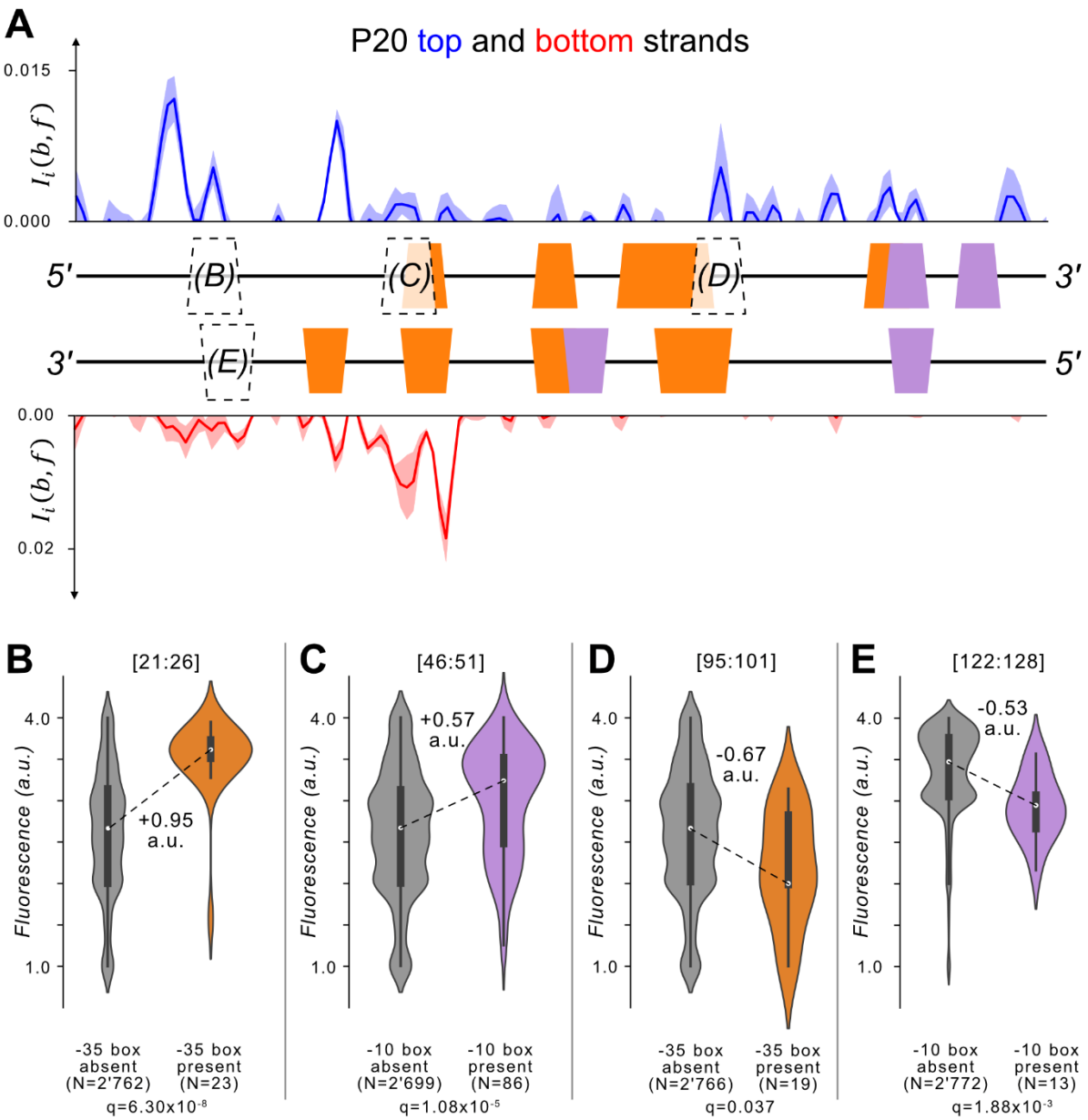

Figure S11. Parent P20. **(A)** We plot the mutual information for the top (blue) and bottom (red) strands of parent P20. Top: the top strand of parent P20. We plot the mutual information $I_i(b,f)$ between nucleotide identity and fluorescence at each position. Solid line: mean mutual information, shaded region: ± 1 standard deviation when the dataset is randomly split into three equally sized subsets (methods). Middle: position-weight matrix (PWM) predictions for the -10 box motifs (magenta trapezoids) and -35 box motifs (orange trapezoids) along the wild-type parent sequence. Outlined trapezoids with letters in parenthesis indicate regions of interest for the subsequent figure panel. Bottom: the mutual information for the bottom strand of parent P20 as described for the top strand. **(B)** We test the null hypothesis that the fluorescence scores have the same central tendency for daughter sequences with vs without -35 boxes at position 21:26 using a two-sided Mann-Whitney U (MWU) test ($q=6.30\times10^{-8}$). The areas of the violin plots are the kernel density estimates (KDE) of each distribution. Within each violin plot is a box plot, where the box represents the interquartile range (IQR) and the white circle the median. Whiskers correspond to 1.5×IQR. **(C)** Analogous to (B) but for gaining a -10 box at position 46:51 (two-tailed MWU test, $q=1.08\times10^{-5}$). **(D)** Analogous to (B) but for gaining a -35 box at position 95:101 (two-tailed MWU test, q=0.037). **(E)** Analogous to (B) but for gaining a -10 box at position 122:128 (two-tailed MWU test, $q=1.88\times10^{-3}$).

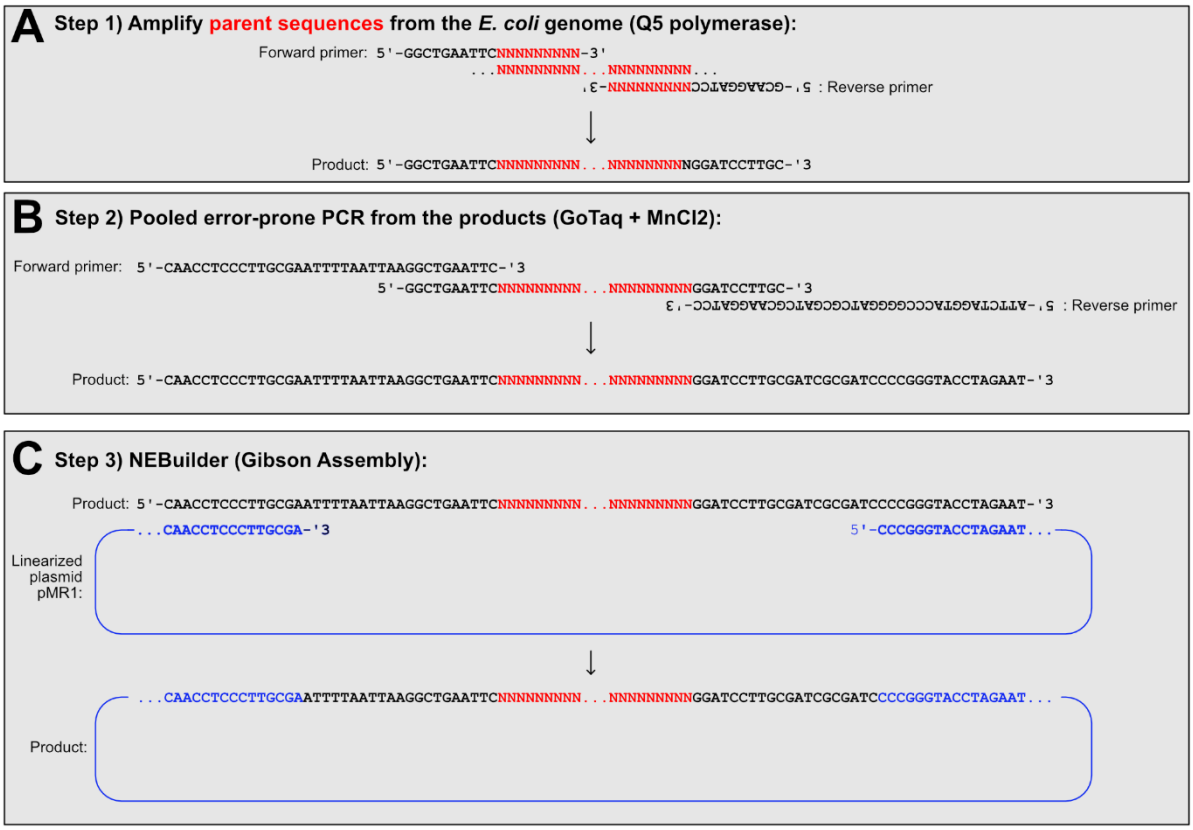

Fig S12. Molecular cloning parent sequences. (A) We first amplify the parent sequences from the *E. coli* genome using Q5 polymerase. Top: the forward and reverse primers contain constant overhang regions, and unique sequences (red N's) unique to the parent sequence. Bottom: the product is a unique parent sequence with the sequences 5'-GGCTGAATTC…insert…GGATCCTTGC-3' concatenated to the flanks. **(B)** We pooled the parent sequences amplified in (A) together for the error-prone polymerase chain reaction using GoTaq and $MnCl_2$. Top: the forward and reverse primers contain constant overhang regions homologous to the pMR1 region for Gibson Assembly. Bottom: the product is the parent sequence flanked by sequences homologous to the pMR1 plasmid. **(C)** We carry out a Gibson Assembly reaction using NEBuilder. Top: we combine the products from (B) with a linear copy of the pMR1 plasmid. Bottom: the final assembly product is the pMR1 plasmid with a mutant library of parent sequences.